79/19

EISCAT
TECHNICAL
NOTE

LECTURES FOR EISCAT PERSONNEL
VOLUME I

by
Kristen Folkestad

KIRUNA
Sweden

LECTURES FOR EISCAT PERSONNEL

VOLUME I

by

Kristen Folkestad
EISCAT
N-9027 Ramfjordbotn
Norway

EISCAT Technical Note 79/19
Printed in Sweden
EISCAT Scientific Association
Kiruna, November 1979
ISSN 0349-2710

CONTENTS

CONTENTS (continued)

1 INTRODUCTION

This report has been compiled from notes prepared for a lecture series given at the EISCAT site at Ramfjordmoen. It is published as an EISCAT document in the belief that parts of it might interest a wider audience.

The intention with the lecturing has been to provide some introductory information of the ionosphere, the incoherent scatter technique and its implementation in the EISCAT observatory for personnel with no prior experience in the space research field. The lectures have been given at rather irregular intervals and represent more of "the spur of the moment" endeavours than a carefully planned, logically organized and balanced scheme. The following two chapters give broad term summary descriptions. More detailed, and partly more mathematical, treatments are found in the subsequent chapters. The ordering of the chapters is somewhat arbitrary.

It will be noticed that the various chapters and sections differ in scope, from providing general background material to dealing specifically with units within the EISCAT technology.

In the areas not covered by this report are topics related to the transmitters, data extraction and data handling hardware. In part these subjects are documented elsewhere (see f.inst. SAC-reports and Proceedings from Abisco-meeting in March 1979). It is felt that it would be worthwhile, though, to try to elaborate more concise expositions of basic working principles and design philosophy. Efforts in this direction may be made in later lectures.

When, in chapter two and three, references are occasionally made to auxillary ground installations in Northern Norway or in Norwegian dependencies in the polar area, this just reflects the fact that the lectures were originally given for the site staff at Ramfjordmoen, incorporating what presumably would be of greatest interest to these employees. The author realizes that there is an expressed need now for a compilation of available characteristics of currently operated ground equipment in all the Nordic associate countries. The appropiate forum for publication of such data would probably be the EISCAT Newletter.

2 IONOSPHERE AND MAGNETOSPHERE

2.1 Definition and charged particle distribution

By definition the Ionosphere is that part of the earth's atmosphere where free electrons are present in quantities sufficient to affect the propagation of radio waves. In practical terms this places the lower boundary of the ionosphere at about 50 km.

This does not mean that the lower reaches of the atmosphere are devoid of charged particles. In fact, positive and negative charges are present in appreciable amounts almost to the ground. However, below 50 km the reservoir of charged species is predominantly made up of negative and positive ions. By collisions, electrons liberated in these lower realms of the atmosphere are almost immediately captured by neutrals to form negative ions. On the average the ionosphere is electrically neutral, implying equal number densities of positive and negative charges.

Due to their relatively large masses the ions remain virtually unaffected by the electrical fields of radio waves traversing the ionosphere, with exception for waves propagating at very low frequencies. The light electrons respond more easily to the oscillating wave fields and are able to influence radio transmissions up to several tens of MHz.

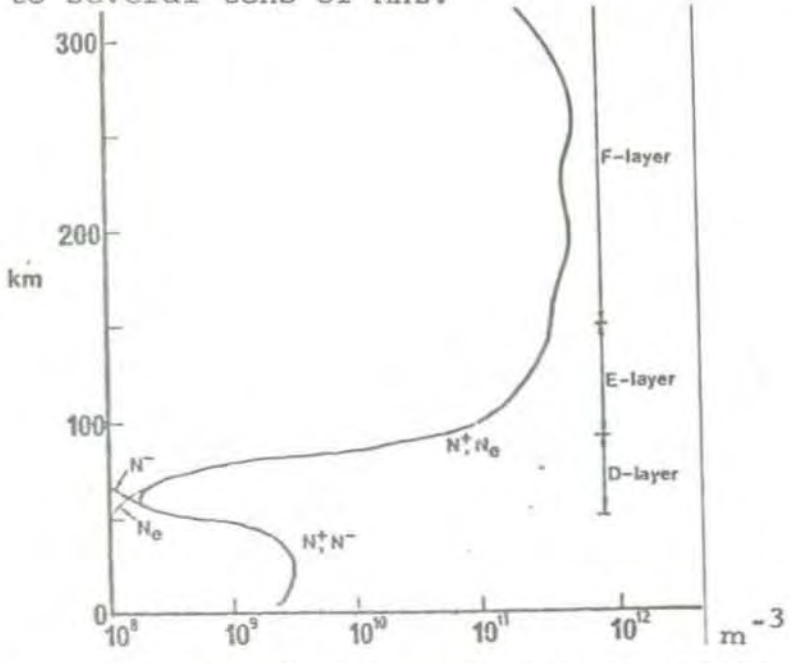

Figure 2.1 Typical distributions of charged species in the earth's atmosphere, N_e denotes electrons N^+ and N^- positive and negative ions respectively

Figure 2.1 depicts a fairly realistic height distribution of free electric charges. It is common to use the symbols D, E, F1 and F2 to distinguish the various parts of the ionosphere. On the upper side the ionosphere merges into the Protonosphere, which is composed principally of ionized hydrogen. (Sometimes the term Heliosphere is used for the height range immediately above the ionosphere, the name derives from an assumed dominance of helium ions. However, observations tend to show that helium ions hardly dominate the ions population at any atmospheric heights.)

Frequently the gas in the upper atmosphere is referred to as a Plasma. In broad terms a plasma is an assembly of particles, some or all of which may be ionized, being everywhere locally neutral on a macroscopic scale under equilibrium conditions.

2.2 Maintenance

It should be noted that figure 2.1 provides no more than an example of possible atmospheric charge distribution. At any height the charge concentration is determined by a dynamical balance involving production and loss mechanisms (under stationary conditions the loss and production terms are equal), and these will vary, often in a rather complicated manner, with altitude, time, geographical position, galactic noise conditions and the solar state.

For any constituent the balance equation may be written:

$$\frac{dN}{dt} = P - L - \nabla \cdot N\bar{V}$$

N: number density
P: production
L: loss
$\nabla \cdot N\bar{V}$: change due to transport

The most important production agency is the photon flux in the X-ray and extreme ultraviolet parts of the solar radiation spectrum, ionizing N_2, O and O_2.

In the high latitude regions electrons and protons of solar origin may acquire sufficient energy to penetrate to ionospheric

levels, and thereby establish an important additional production source. The charge population below the ionosphere is maintained by energetic galactic radiation.

Ionization is lost by various recombination processes, among which the dissociative recombination mechanism may be the most important. In this kind of ion-electron encounter a molecular ion is fractionized into neutral atoms, which may be left in excited states. In the higher regions of the ionosphere, say above 200 km, transport of charges may contribute significantly to the ionization balance. The transport processes are of different origin, associated with diffusion and winds driven by tidal motions and by thermal atmospheric expansions and contractions.

2.3 Ion composition

Mass spectrometer measurements conducted during the last 10-15 years have disclosed an extremely complicated ion composition in the ionospheric D-region. Up to 80-85 km the positive ion assembly is frequently found to be dominated by hydrogen compounds of the type $H^+ \cdot (H_2O)_n$. Above the hydrated ion regime, and throughout the entire E-region, molecular oxygen and nitric oxide ions, O_2^+ and NO^+, are the principal positive constituents. O^+ becomes the most abundant ion above 150-225 km.

At high altitudes a transition from O^+ to H^+ dominance will occur. At which level this transfer actually takes place, is partly a matter of speculation. It has been conjectured that an outflow of H^+ along the geomagnetic field lines will be established in the polar cap regions. This will increase the altitude for the O^+/H^+ transition, possibly by several thousand kilometers. The outflow of H^+, known as the Polar wind will be one of the experimental topics to be addressed with the EISCAT facility (Blanc, 1977).

2.4 Temperatures and collision frequencies

As in most gaseous substances the charged and neutral atmospheric particles are in a state of incessant random motion. Assuming that the velocity distribution for a particular gas component is Maxwellian, a temperature may be defined in terms

of the average kinetic energy: $E_{av} = 3/2\ kT$, where k is Boltzmann's constant.

In the upper ionosphere, above the lower part of the E-layer, thermal equilibrium is generally not attained, and the electron, ion and neutral gases will have to be ascribed different temperatures.

Electrons liberated in an ionization process will carry a part of the excess energy of the ionizing photons or particles. Since energy exchange is particularly effective amongs particles of equal masses, thermalization may proceed quickly enough to maintain the Maxwellian velocity distribution. Due to this selective heating of the electron population, we generally have $T_e \geq T_i \geq T_n$.

In the D-region, and throughout much of the E-layer, collision frequencies are high enough to prevent notable temperature differences to be maintained, at least for extended periods of time. Good thermal contact between ions and neutrals remains even after the electron temperature starts to deviate from the neutral temperature at 150-200 km. However, with the increasing rarefaction in the upper reaches of the atmosphere the ion-neutral thermal contact will deteriorate with altitude, and finally the ion temperature approaches the electron temperature again.

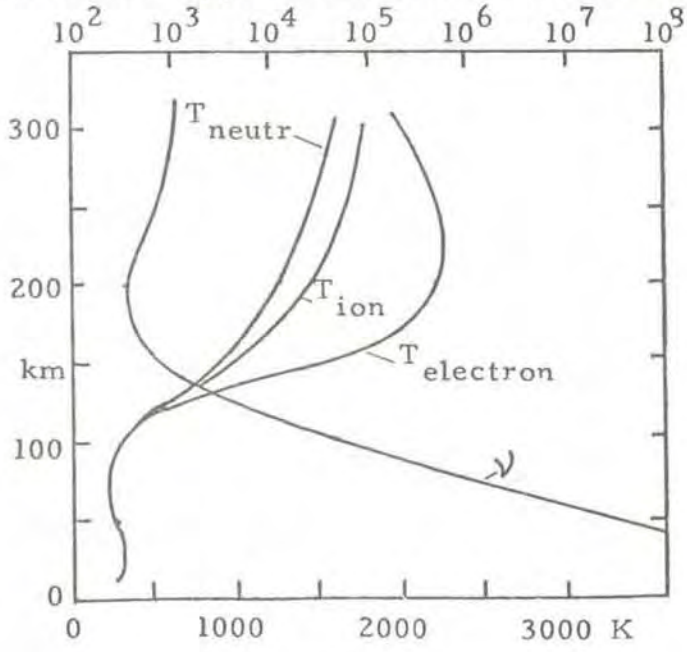

Figure 2.2 Characteristic daytime variations of the temperatures of charged and neutral atmospheric species, along with a display of the height dependence of the effective electron collision frequencies

Figure 2.2 shows a realistic height variation of daytime temperatures. It should be noted that the T_e/T_i ratio is a variable quantity, ordinarily attaining its minimum value (often close to 1) at night hours.

Electron-neutral collision frequencies are important for radio wave propagation at low and intermediate frequencies, determining the wave attenuation by momentum transfer to the neutrals. A height profile of effective electron collision frequencies is included in figure 2.2. It is seen that the electron-neutral collisions decrease rapidly with height, tending to make their effects on propagating waves insignificant above the D-region.

For incoherent scatter observations the effect of collisions may be appreciated by examining the ratio of the exploring wavelength to the mean free paths. Since the mean free path of the electron is roughly an order of magnitude larger than the mean free path of the ions, it turns out that the ion-neutral collisions are more significant than electron-neutral encounters for these kind of measurements (Evans, 1969).

A plasma parameter of particular importance for incoherent scatter relations is the electron Debye length, given by the expression $\Lambda_D=6.9\sqrt{\frac{T_e}{N}}$, where T_e is the electron temperature and N the electron density, per cm^3. Throughout most of the ionosphere, with exception for the lowest and highest regions, the Debye length will remain less than 1 cm.

In a sheat surrounding a charged body in an ionized gas there will be an excess charge of polarity opposite to the body charge, sufficient to balance the charge on the body. The Debye length is a rough measure of the dimension of the sheat. Sometimes the Debye length is referred to as the screening distance, implying that the electric field caused by the charged body is not felt at larger distances.

2.5 Geomagnetic field configuration - the Magnetosphere.

The earlier concept of a dipole-like geomagnetic field stretching into the vacuum of the interplanetary space has been replaced by a model sketched in figure 2.3.

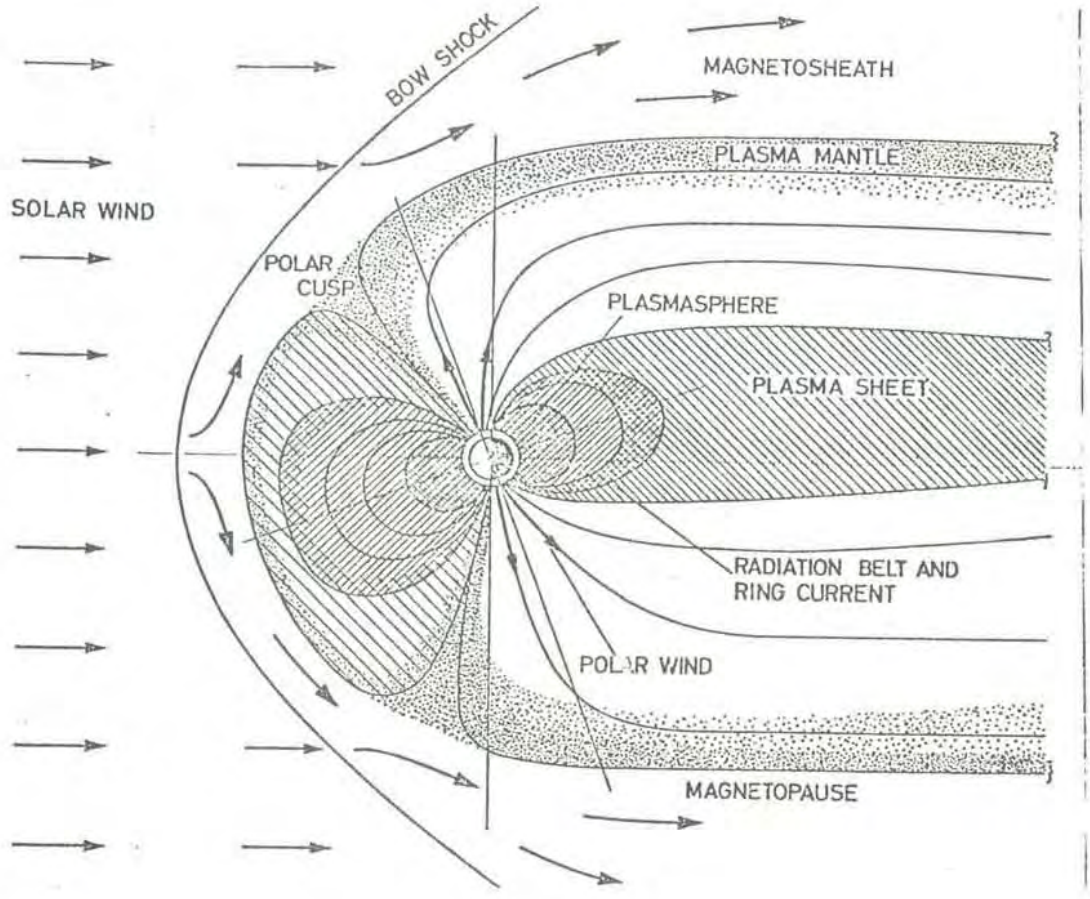

Figure 2.3 Magnetospheric model (Akasofu, 1977)

The main features of this model have been disclosed by numerous satellite missions. The earth's magnetic field represents an obstacle to the Solar Wind, the continous, but highly variable, stream of supersonic particles emanating from the sun. A collision free shockfront is formed as a result of this interaction, confining the sunward portion of the Magnetosphere. In the geophysical parlance the outer bordery of the geomagnetic field is known as the Magnetospause.

On the sunlit side the geomagnetic field is compressed; the distance to the field border is here of the order of 10 earth radii. In the anti-solar direction the field forms an extended cylindrical cavity with a magnetically neutral core. It is common to refer to the cylindrical cavity beyond about 10 earth radii in the anti-solar direction as the Magnetotail. It may be noted that currents have to flow on the boundary surfaces and across the tail to maintain the displayed magnetic field configuration.

The true nature of the magnetic field structure behind the bow shock and at the magnetospause is still a matter of contemporary conjecture and discussions. Further experimental investigations of this topic may be regarded as today's "taks number one" of magnetospheric physics (Roederer, 1977).

The Open Magnetosphere model, regarded by some physicists as necessary to explain the assembly of observational data (Akasofu, 1977), prescribes a field line topology schematically shown in figure 2.4.

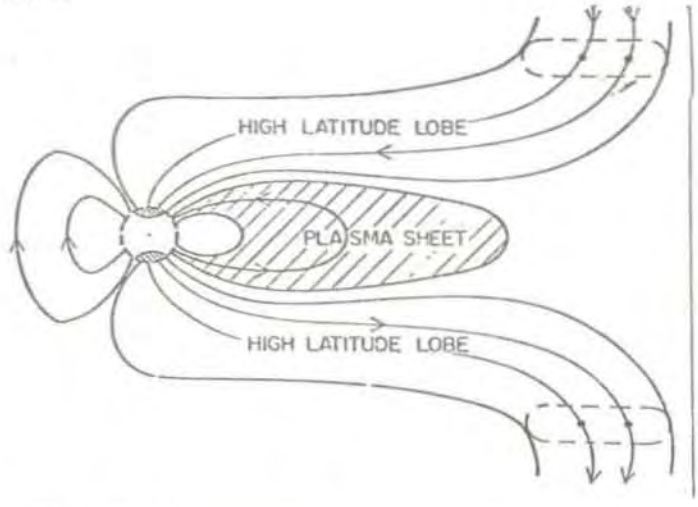

Figure 2.4 Open field line model

In this model the field lines permeating the High Latitude Lobe merge with the interplanetary magnetic field, forming an access rod road for the interplanetary plasma into the polar regions of the magnetosphere/ionosphere. It has been maintained that the electric energy neccessary to drive currents in the magnetosphere/ionosphere system is provided by a concersion of kinetic solar poarticle energy to electric energy in the plasma moving across distant portions of the open field lines.

In the Closed Magnetosphere model the perpendicular component of the magnetic field is zero everywhere on the magnetospause and plasma can only enter the magnetosphere by diffusion through the magnetopause or by flowing through boundary neutral points.

The Electric Field Configuration in the magnetosphere is a rather complex topic. Suffice it to state here that all published theories generally seem to indicate the presence of a

large scale dawn-to-dusk field of some tens of kV.

The magnetosphere may be looked upon as a dynamical system with domains of particles posessing a wide range of different energies, continously moving under the influence of existing force fields.

The equation describing the particle motion is given by:

$$\frac{d}{dt}(m\frac{d\bar{r}}{dt}) = q(\frac{d\bar{r}}{dt} \times \bar{B} + \bar{E}) + \bar{F} \qquad (2.1)$$

where $\bar{r}$ is the position vector. $\bar{B}$ the magnetic induction, m the particle mass $\bar{E}$ and $\bar{F}$ the electric and nonelectromagnetic forces respectively.

The general solution of this equation is complex. But under certain conditions of field geometry, particle energy and external force fields, periodicities appear, allowing for simpler descriptions.

There may be three distinct types of periodicities: (i) the cyclotron motion, a periodicity in the motion transverse to the magnetic field, (ii) the bounce motion, a periodic motion up and down the magnetic field lines and, (iii) the drift motion, a periodic motion along closed surfaces made up of field lines. Cyclotron frequencies are orders of magnitude higher than the bounce frequencies, whereas drift frequencies are orders of magnitudes lower than the bounce frequencies. With no acceleration of the particles along the magnetic field lines, the quantity $\sin^2\alpha/B$, where α is the switch angle, the angle between the velocity vector and the field direction, remains constant. With an increase of $\bar{B}$ at the lower altitudes the pitch angle increases. Mirroring takes place for $\alpha = 90^o$.

With no external forces present the drift motions in the magnetosphere are created by the inhomogeneity in the magnetic induction and by centrifugal forces created by field line curvatures. Electrons are drifting eastward and protons westward (figure 2.5).

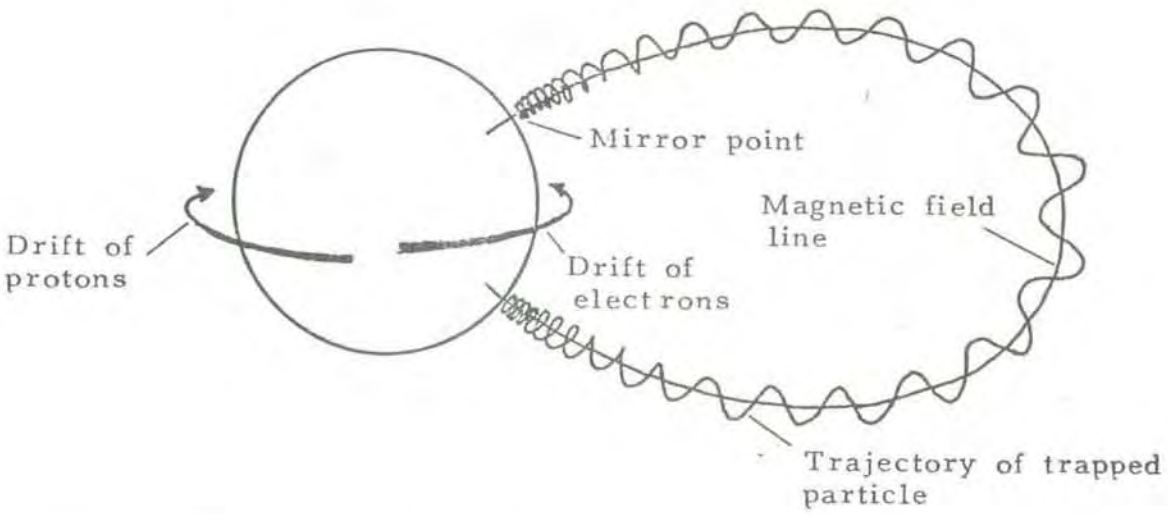

Figure 2.5 Drifts of trapped species

Under certain conditions one is justified in regarding the drift as confined to fixed L-shells. L is a dimensionless parameter, which in a dipole model simply specifies the equatorial distance to a particular field line, in terms of earth radii. The Invariant Latitude, Λ is defined by the relation $\cos^2\Lambda = L^{-1}$. λ defines the latitude at which a field line of parameter L intersects the earth's surface. Particles whose drift shells are closed around the earth are said to be Stably Trapped. Particles drifting on field lines with their equatorial points at distances less than about $8R_e$ (earth radii) usually belong to this category.

Particles moving on field lines at larger equatorial distances are subject to an azimuthal convection, under the influence of the prevailing electric field, causing the flux tubes to intercept the magnetopause. The notion of "frozen-in field lines" is commonly used to describe this kind of behaviour. This involves that the field lines are considered to move with the plasma. Upon reaching the magnetospheric boundary, the field lines open and merge with the interplanetary field. Subsequently the magnetic lines are dragged by the solar wind across the polar cap and added to the outside of the magnetic tail. Field lines and plasma are then convected to the neutral sheet, where the lines reconnect and collapse to a dipole like form. (The validity of using the concepts of "frozen-in field lines" and "field-line reconnection" is seriously questioned by Alfvén (1976). It is beyond the scope of this presentation

to delve deeper into this interpretation. The feature to be emphasized here is that forces exist, causing large scale movements of the magnetospheric plasma). As will be noted from equation 2.1 the significance of the electric field for the drift behaviour of a particle depends upon the particle's energy. For low energies the electric field tends to dominate, driving both protons and electrons in the same direction. For high energies the particle drifts caused by electric fields may be significant.

Some main features and key notions of the magnetosphere are described in a summary fashion in the following:

1. The Radiation Belts (sometimes referred to as Van Allen Radiation Belts) are domains of trapped electrons and protons of energies from a few keV to several MeV, occuring for $L < 6$ to 8. The most energetic particles are found in the Inner Belt (for L 2 to 3). The minimum flux region between the Inner and Outer Belts is referred to as the Slot Region. It is now believed that during disturbances particles from the outer zone may be released by wave-particle interaction, and subsequently penetrate to the lower regions of the ionosphere, creating enhanced auroral activity and increasing the number densities of thermal charges.

2. The Plasmasphere is the inner relatively dense and cold part of the magnetosphere, where the plasma and the magnetic field lines are considered to rotate with the earth. The boundary surface, on the average positioned at about L=4, is denoted the Plasmapause. Outside the plasmapause the particle motion is influenced by convection. Reductions in ion densities of more than two orders of magnitude have repeatedly been observed in satellites moving through the plasmapause from lower to higher altitudes.

3. The Polar Wind is the outflow of H^+ along high latitude field lines. It has been conjectured (Banks, 1972) that the outflow may take place not only on open field lines, but essentially on all lines convecting outside the plasmapause.

4. The Polar Cusp is the region on the dayside magnetosphere where the field lines leading up from the earth appear to touch the magnetopause. In the region of contact at the magnetopause the magnetic field intensity is extremely low. Plasma in the cusp has been found to have essentially the same energy properties as the plasma in the Magnetosheath, the region between the bow shock and the magnetopause. The field lines of the cusp region map into the ionosphere at the dayside of the so-called Auroral Oval, an oval-shaped belt delineating the maximum occurence of visual auroral arcs.

5. The Plasma Sheet is a relatively thin layer of plasma bisecting the cylindrical magnetotail into a northern and a southern half. The plasma density in the sheet is typically of the order of 0.1 cm^{-3}. There is experimental evidence that the plasma sheet serves as a reservoir of particles creating diffuse auroral displays along the night-time part of the oval. During disturbed periods plasma sheet particles may be accelerated and give rise to discrete auroras. Furthermore, at time of disruption accelerated plasma sheet particles may penetrate into the outer radiation belt and become part of the trapped population.

6. Outside the plasma sheet is the Plasma Mantle. The plasma in this region has magnetosheat-like energy spectra and flows in the anti-solar direction.

7. It has been established as a regular feature of the magnetosphere (Bostrøm, 1977) that sheets of Field Aligned Currents flow into ionosphere at auroral oval latitudes. On the morning side of the oval the current flows into the ionosphere along the poleward border and out of the ionosphere along the equatorward side. On the evening side of the oval the flow directions with respect to the borders mentioned above are reversed. In the ionosphere the circuits are closed by currents flowing transverse to the magnetic field lines. The charged particle transport along the oval is usually referred to as the Auroral Electrojet.

8. Magnetic Substorm is the notation given to a composite class of phenomena occuring as a result of the release of energy accumulated in the magnetosphere. The energy discharge is thought to be triggered by a change in the interplanetary magnetic field vector (IMF). It has been held that each magnetic substorm is immediately preceded by a southward turning of the interplanetary field vector, but this hypothesis is discarded by Akasofu (1977). A magnetic substorm affects almost all the major parameters in the magnetosphere/ionosphere system. Characteristic substorm manifestations are: disturbances in magnetic field measurements on the ground, enhanced auroral activities, increased ionizations in the lower ionosphere caused by precipitating particles, a contraction of the plasmasphere, a rechannelling of a part of the cross-tail current, causing enhanced current flow along the field lines into the oval ionosphere and a following expansion of the auroral electrojet.

It will be evident from the foregoing that the polar regions, especially the equatorward demarcation zones, the auroral ovals, are particularly important vantage fields for studies of the complex relationships which govern the dynamics of the magnetosphere/ionosphere composite system. The recognition of this fact has been the main incentive in the efforts leading up to the establishment of EISCAT.

References

Akasofu, S-I - Physics of Magnetospheric Substorms, D Reidel Publ. Comp (1977)

Alfen, H - J Geophys Res 81, 4019 (1976)

Banks, P - In: Magnetosphere-Ionosphere Interactions, Ed K Folkestad, Universitetsforlaget (1972)

Blanck, M - In: Radar Probing of the Auroral Plasma, Ed A Brekke, Universitetsforlaget (1977)

Evans, J V - Proc IEEE 57, 496 (1969)

Roederer, J - Space Sci Rev No 2 (1977)

3 SUMMARY OF EXPERIMENTAL TECHNIQUES

In this chapter we intend, for the purpose of providing some appropriate background information, to present a brief summary of tehcniques which have been employed in exploring the ionosphere and the more remote parts of the earth's environment.

3.1 Radio wave observations on the ground.

3.1.1 Vertical soundings

The Ionosonde has been the "workhorse" in experimental ionospheric physics for more than 50 years. In principle the ionosonde is a radar transmitting vertically directed pulsed signals, in the frequency range from a few hundred kHz to 10-20 MHz. The time of travel $|\Delta t|$ of signals reflected from the ionosphere is recorded and a Virtual Reflection Height is determined by assuming that the signals propagate with the velocity of light, $h' = \Delta t \cdot c/2$. From magnetoionic theory we know that a signal is reflected from that level in the ionosphere where the exploring frequency equals the Plasma Frequency, f_N related to the electron density N by the simple expression $f_N^2 = 81\ N$ (f_N in kHz for N in electrons per cm^3).

By increasing the frequency the wave will penetrate deeper into the ionosphere to meet the reflection condition. The maximum frequency reflected is termed the Critical Frequency for the particular layer explored. This corresponds to the maximum electron density in the layer. Frequencies above the critical frequency pass through the layer and are either reflected by higher layers of disappear into space.

By sweeping through the reflection range a virtual height/frequency relationship, known as an Ionogram is obtained.

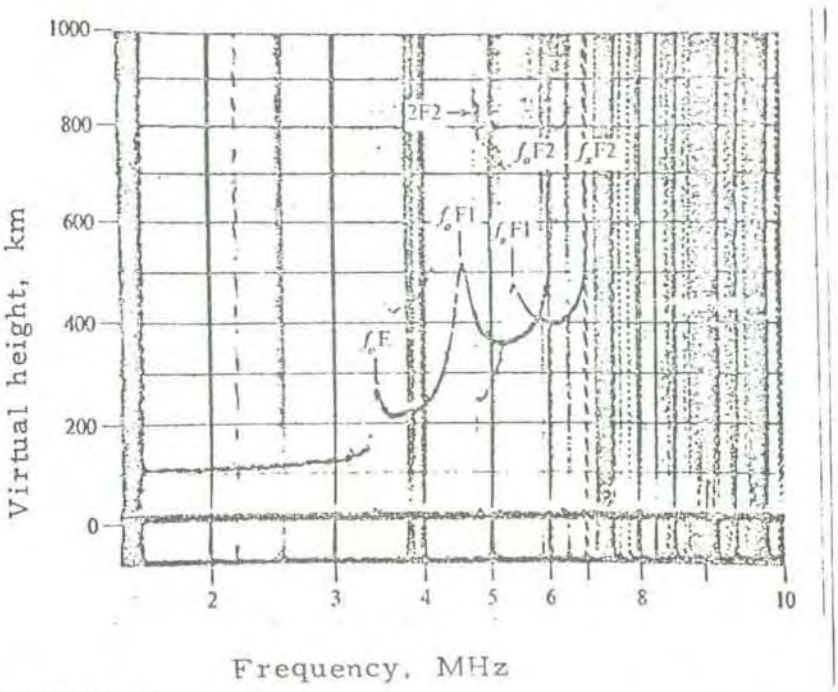

Figure captions:

Figure 3.1 Ionogram showing ordinary and extraordinary F-layer traces in addition to E-layer returns

Figure 3.1 gives an example. Frequencies close to the critical frequency suffer large group retardations in the ionosphere, manifest in the ionogram in the increase in the virtual height recorded. Procedures have been designed for converting the ionograms to true height/electron density profiles.

In a strict sense the presentation given above is incomplete. As a result of the presence of the earth's magnetic field an upgoing wave upon entering the ionosphere will generally be split into two elliptically polarized components with opposite hands of rotation.

The two components, termed the Ordinary and the Extra-ordinary waves, travel with different velocities, and are reflected at different height levels. The description given above applies to the ordinary component. Traces of both components will generally appear in an ionogram.

For the ordinary mode the ray path will be bended towards the magnetic field in the manner shown in figure 3.2 (We assume for simplicity that the magnetic field vector is in the plane of the paper.)

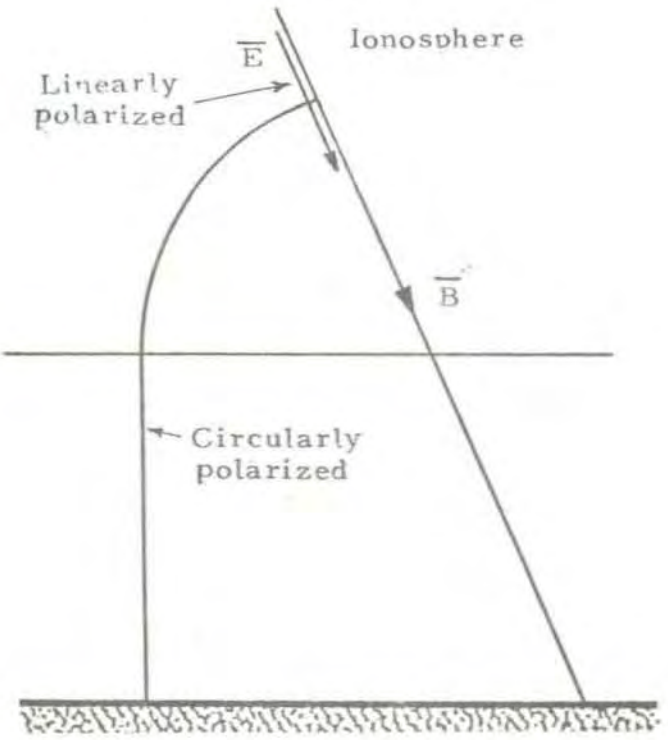

Figure 3.2 Ray path of ordinary wave

As the wave propagates the polarization changes from circular at the bottom of the ionosphere to elliptical. As the reflection point is approached, the polarization ellipse degenerates into a line. Reflection takes place at X=1 ($X=f_N^2/f^2$). Here the wave is linearly polarized with the electric field vector along the magnetic field.

It is noted that the reflection condition depicted in figure 3.2 is of primary importance for the "Heating"-experiment, to be implemented by Max-Planck-Gesellschaft adjacent to the EISCAT-installations at Ramfjordmoen. One of the main objectives of this experiment will be to study instabilities created by a powerful ordinary wave component at X=1.

As will be clear from the foregoing, the principal parameter to be studied by vertical soundings is the electron density and its variation with height. Information about dynamic behaviours may be derived by analysing time sequences of ionograms taken at convenient time intervals. A clear limitation in this kind of technique is that it only samples the bottom side of the ionosphere.

A modern type of ionosonde, developed at the University of Tromsø, will be installed close to the EISCAT transmitter site. The ionograms are expected to be of value in normalizing

electron density profiles derived from the scatter observations, and also for experiments requiring electron density information for technical pre-adjustments of the EISCAT setup (f inst for measurements of the so-called plasma lines).

3.1.2 Oblique soundings

Ray paths for transmissions at oblique angles are depicted in figure 3.3.

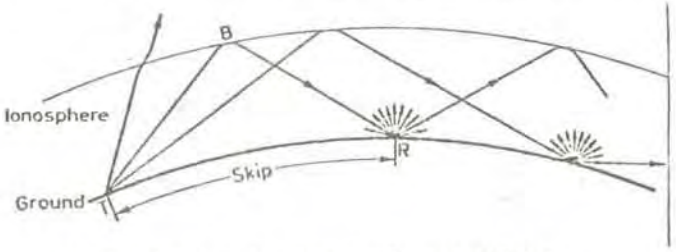

Figure 3.3 Geometry of ground scatter

With a horizontally statified ionosphere the signals which in this case may be detected at the transmitter location stem from the tiny fraction of energy scattered in the backward direction where the wave hits the ground. The record will be in the form of a trace branching off the second hop vertical trace for the layer sustaining transmission (we assume that sufficient energy leaks off in the vertical direction to permit the vertical ionogram to be observed).

Irregularities, in the sense of regions with electron densities deviating from the background medium, may give rise to direct ionospheric echoes also in oblique soundings. In particular echoes may be noted from field alongated irregularities, located where the wave impinges on the field lines at approximately right angles. Drift motions of irregularities at auroral latitudes over the North of Scandinavia are currently being studied in the STARE project, operated by Max-Planck-Institut, Lindau (STARE-Scandinavian Twin Auroral Radar Experiment). This facility includes two multibeam radars, located near Trondheim and Sauvamaki (Finland), working at frequencies close to 140 MHz.

3.1.3 D-region measurements

Since the traces of an ionogram are caused by reflections at E- and F-layer heights, little or no information about the ionospheric D-region can be derived from these measurements.

One technique which has been applied fairly extensively in the passed to study D-layer absorption uses the amplitudes of multi-

hop echoes. A calibration factor is derived by recording the reflected echoes at night hours, when the absorption is low.

An alternative technique for D-region absorption studies makes use of a Riometer (relative ionospheric opacity meter) for measuring the intensity of cosmic noise emissions. The directional source is assumed to remain constant. Superposed on diurnal variations in the received noise power, created by the rotation of the earth-fixed antenna beam over the sky, are changes in the attenuation suffered by the radiation on its passage through the D-region. Changes in the absorption of 0.1 dB can usually be recorded with such an instrument, operated at a frequency close to 30 MHz. Calibration is carried out by periodically disconnecting the antenna and feeding into the receiver a known amount of power from a noise diode. Observation of extraordinary high absorption by riometers at high latitudes are usually indicative of an enhancement of the radiation flux of preciptitating high energy particles.

Riometers working at 30 and 40 MHz are presently operated at Ramfjordmoen, Ny Ålesund (Spitzbergen) and the Bear Island by Dansk Meteorologisk Institutt. In future a similar set of riometers may also be installed at Jan Mayen. Max-Planck-Institut, Lindau, runs another riometer at 50 MHz at the Ramfjordmoen site.

Other experimental methods used for D-layer studies are based on the Cross Modulation ("Luxembourg") effect and observations of Partial Reflections. An established procedure for the application of the first technique has been described by Thrane (1966). A "wanted" pulsed signal is transmitted with a pulse repetition frequency p. By transmitting synchronized "disturbance" pulses at half the repetition rate, p/2, each other wanted pulse is exposed to a heating effect created by the disturbing signal. By measuring the undisturbed and disturbed wanted pulses and using available theory, electron densities and effective collision frequencies may be deduced.

The partial reflection method relies on weak reflections from small discontinuities in the lower ionosphere as a wave penetrates the region. The ratio of the amplitudes of the scattered signals of both the ordinary and the extraordinary components is measured. By combining this measured quantity with the ratio of the reflection coefficient and absorption indices, deduced from generalized magnetoioric theory, the electron density may be computed.

A partial reflection experiment is operated by the University of Tromsø at Ramfjordmoen site area. The data handling is computerized to give D-region height/electron density profiless almost in real time. There are plans for supplementing the existing installation with phase - measuring equipment to facilitate a derivation also of collision frequencies.

It should be mentioned that electron densities and collision frequencies in the D-region have also been investigated by studying phases and amplitudes of waves actually reflected in the D-layer, ranging in frequency from 10 to 200 kHz, propagated over distances of up to 1000 km. The height distributions are derived by "trial and error" as those giving the best fit to the observations.

3.1.4 Faraday rotation method.

In an earlier section we have mentioned that a linearly polarized wave generally splits into an ordinary and an extraordinary component upon entering the ionosphere. For reasonably high frequencies (above a few MHz) and an approximately vertical magnetic field the two components are propagating in the so-called quasi-longitudinal mode, implying that they are circular polarized. Since the two waves travel with different velocities the plane of the resulting linearly polarized wave rotates gradually. This phenomenom is known as Faraday rotation. The total rotation is a measure of the total columnar electron content between the observing location and the source.

The Faraday rotation method has been applied to study the total columnar electron content of the ionosphere by using signals from artificial satellites and moon-reflected echoes.

The method has also become a standard technique for deriving electron densities in the lower ionosphere in conjunction with rocket launchings.

The plane of the electric resultant field is continuously detected by antennas carried on the rocket. By keeping record of the rotation from the bottom of the ionosphere, the rotation angle may be plotted as a function of distance. The derivative of this curve at any distance is proportional to the electron density.

3.2 Magnetic observations

The main component of the geomagnetic field is caused by currents flowing in the interior of the earth. Regular and irregular variations are created by currents flowing in the ionosphere/magnestosphere, and currents induced by these charge transports in the upper atmosphere.

Precipitating particles play an important role in generating atmospheric currents at high latitudes, particularly in the auroral oval. Estimates have been quoted that the auroral electrojet under disturbed periodes may rise in intensity to 10^6 Amps.

A Magnetometer is an instrument designed to measure the geomagnetic field and its variations. Normally a ground based magnetometer is constructed to observe the north-south, east-west and vertical component of the field vector. Similarities in the patterns observed during particular types of disturbances make it possible to use the magnetometer records as an indicator that certain types of events are under development. F inst are magnetometer observations essential in diagnosing the onset and the major phases of magnetic substorms.

In Norhern Norway magnetometers of the flux gate type are operated at Tromsø, Ramfjordmoen, Skibotn, Ny-Ålesund, Beer Island and Jan Mayen.

3.3 Optical measurements

Much efforts have been made during the last two decades to study in considerable detail the optical emissions from excited

neutrals and ions in the ionosphere. The most intense radiations are generated in the lower portion of the E-region. Some emissions are observable to the naked eye, others are outside the visible range. There have been particular interest for observing certain lines or bands in the spectrum, such as the ionized nitrogen bands at 3914 and 4278 Ångstrøm and the green and red oxygen lines at 5577 and 6300 Ångstrøm. The intensities of the nitrogen emissions are believed to be proportional to the production of ionization by particle bombardment. The 6300 Ångstrøm line may be an indicator of the F-region recombination rate.

A common device for optical observations is the All-Sky Camera, surveying the whole sky above the observing location. Refined TV cameras are used for resolving fine scale variations in the auroral forms. Ground based optical tracking of rocket released barium clouds have been used to derive electric fields in the ionosphere.

4 channel scanning photometers covering Hβ-emissions and the three upper wavelength regions mentioned above are in current use at the Skibotn field station. In addition Dr. Lauche at the Max-Planck-Institut, Lindau, will implement a panoramic photometer covering the same wavelength interval at Ramfjordmoen. Routine measurements with an all-sky camera are made at the University of Tromsø.

3.4 In-situ investigations

Under this heading we group experiments conducted on sounding space vehicles, satellites and rockets and, to some extent, on balloons.

In terms of instrumentation there is hardly any reason to distinguish sharply between rockets and satellites. Rocket and satellite payloads are often equipped to measure essentially the same parameters. In the way of operation we may note significant differences, though. A satellite may provide global coverage whereas a rocket is exploring a more limited region of the ionosphere. On the other hand, a satellite is bound to follow the elliptical orbit into which it is put by

launch. Data acquisition on bord a satellite is therefore not controlled to the same extent as is the data collection on a rocket, which usually is launched only in the presence of a certain set of preselected geophysical events. The speeds of the two kinds of space vehicles are notably different. A velocity of 10 km/s may be typical for a satellite, whereas 1-2 km/s is more characteristic for a rocket. Whether high speed shall be regarded as an asset or not, depends upon the nature of the experiment. High speed will be an advantage for the ability to measure with good/spatial resolution. If good time resolution is of prime importance, the high-speed behaviour is a clear disadvantage. Even with the more slowly moving rockets it may, at times, be a problem to distinguish between spatial and temporal variations. Both kinds of vehicles have their special areas where their superiority is unprecedented. F inst mass spectrometry in the ionospheric D-region can only be conducted on rockets; the uppermost part of the ionosphere, the magnetosphere and our interplanetary space are only accessible for direct measurements by satellites. It will be outside the scope of this brief presentation to deal in any detail with the details of airborne experiments. Suffice it to list some of the more common techniques:

1. Various kinds of electrostatic and RF-probes are widely employed to provide electron temperatures and densities of electrons and positive ions. Ionization structures with dimensions of a few hundred meters, sometimes even less, may be resolved in these kinds of observations.

2. Electric fields along pre-selected axes are investigated by observing the potential differences between identical electrodes sufficiently separated to be undisturbed by each other and by the vehicle.

3. Particle fluxes, ranging in energy from a few eV, or tens of eV, to several hundreds of keV are detected by arrays of particle counters. Directional properties, commonly referred to the magnetic field direction, are determined by combining the instrument's mounting geometry with the vehicle's spinning motion and magnetic aspect data.

4. Multiaxial magnetometers are key instruments for mapping the magnetic field and for studies of the currents causing the observed magnetic field structures.

5. A rich complement of optical instruments are used in airborne applications, such as photometers, sensible to various parts of the spectrum, UV and X-ray sensors, TV and all-sky cameras. A particularly important field of investigation is the mapping of auroral arcs and arc systems. Details are brought out by rockets flying through or close to, the arcs. Satellite pictures taken at remote distances may provide excellent snapshots of the visual displays att along the auroral oval.

6. Data on the composition of the neutral and ionized parts of the atmosphere are furnished by mass spectrometer measurements. Particular efforts are required in D-region spectrometer applications. These arise from the need, at these relatively dense part of the atmosphere, to evacuate the instrument to ensure that reactions among the sampled species are not taking place within the spectrometer itself.

A variety of airborne radio measurements have been reported, in addition to the Faraday technique mentioned in an earlier section. Amongst the applied methods arc top-side swept frequency soundings (similar to the sounding technique applied on the ground to obtain bottom-side ionograms), recordings of ground transmitters, particularly at VLF frequencies, passive listening for radio emissions generated by natural processes.

In recent years several active experiments have been flown, where accelerated particles are injected into the ionosphere, modifying the particle population close to vehicle, creating optical emissions and generating various kinds of radio waves. Wave propagation experiments with both the transmitter and the receiver inside the ionosphere, but a different locations, in a split-payload configuration, have also been conducted. A general finding in these experiments is that electrostatic waves play a very important part in the observed transmissions. These are space-charge waves which cannot be directly observed

outside the ionosphere (they may be indirectly detected, though, f inst in their signatures left on incoherent scatter spectra). It is expected that much of the funds available for in-situ measurements in US and in Europa in the 1980's will be allocated to the Space Shuttle missions, an experimental project jointly planned and operated by NASA/ESA (ESA-European Space Agency). The shuttle orbiter is a manned aircraft,approximately the size of a DC 9 jet liner, designed for reusable performance. It will be carried aloft by boosting rockets. stay in orbit for some days, and thereafter land as a glider. The vehichle will carry a manned laboratory, the Spacelab, and be equipped to extend experimental techniques applied so far on satellites and rockets.

Balloons have been exwidely used for studying particle fluxes with energies above 40 keV, by detecting bremsstrahlung X-rays generated by these particles in their interaction with the upper atmosphere. Typical balloon altitudes are 30-40 km, the active measuring phase sometimes extending over several days. Balloons are also applied for observing electric fields mapped downward from the ionosphere. Only large scale fields, with scale size above 400 km, may be studied by this technique.

References

Thrane, E V - NDRE Report No 54 (1966)

4 BASICS OF THE INCOHERENT SCATTER TECHNIQUE

4.1 Introduction

In 1958 Gordon postulated that radio technology had advanced to a stage where it should be possible to use the incoherent scatter technique for ionospheric diagnostics. Although disagreeing in some detail, experiments conducted during the succeeding 20 years have essentially substantiated Gordon's predictions. Today incoherent scatter observations have an established reputation for offering the most versatile technique of all ground-based methods used to explore the upper atmosphere.

In this chapter we will outline some features of the theory for the scattering of electromagnetic waves in the ionosphere.

4.2 Theory

We assume that the transmitted frequency is far above the ionospheric plasma frequencies (which allows us to disregard refraction and group retardation). During its passage through the ionosphere the transmitted wave imparts to the electrons an oscillatory movement which in turn gives rise to a radiation field of electromagnetic energy. With the observer sufficiently far from the scattering volume, only the far-field radiation component needs to be taken into account. For the field from the single electron, received at a distance R_s from the scatter location, we may write:

$$\bar{E}_s = \frac{q}{4\pi\varepsilon_o c^2} \frac{\bar{R}_s \times \bar{R}_s \times \dot{\bar{v}}}{R_s^3} e^{-i\bar{k}_s \cdot \bar{R}_s} \qquad (4.1)$$

where q denotes the electron charge, $\bar{R}_s$ the radius vector from the scatterer to the field point and $\dot{\bar{v}}$ is the acceleration of the oscillating charge. k_s is the wave vector in the direction of the observer. The phase factor $e^{-i\bar{k}_s \cdot \bar{R}_s} = e^{-i\omega_o R_s/c}$ has to be included to account for the fact that the field observed at the given location at time t was actually radiated by the source at time $t - \frac{R_s}{c}$.

The acceleration of the charge may be derived from the equation of motion:

$$\dot{\bar{v}} = \frac{q}{m_e} \bar{E}_o e^{i(\omega_o t - \bar{k}_o \cdot \bar{R}_o)} \qquad (4.2)$$

ω_o is the angular frequency of the transmitted wave, m_e electron mass and $\bar{E}_o$ the complex amplitude of the wave incident upon the scattering medium. $\bar{k}_o$ is the wave vector of the incoming wave.

By combining equation (4.1) and (4.2) the observed field may be written (an immaterial phase factor has been omitted):

$$E_s = r_e E_o \sin\xi \frac{e^{i \omega_o t}}{R} e^{-i(\bar{k}_o - \bar{k}_s)\cdot \bar{r}} \qquad (4.3)$$

Here R is the distance from the centre of the scattering volume to the observer, $\bar{r}$ the radius vector from the centre to the position of the oscillating charge. ξ is the angle between the electric field vector of the incident wave and the direction of scattering. Assuming $|\bar{k}_o| = |\bar{k}_s|$ we have:

$$\bar{k} = |\bar{k}_o - \bar{k}_s| \hat{k} = 2k_o \sin\Phi \hat{k} \qquad (4.4)$$

where $\hat{k}$ is the unit vector along the bisector of the angle between the radius vectors from the scatterer to the transmitter and observer; r_e is the classical electron radius:

$$r_e = \frac{q^2}{4\pi \varepsilon_o c^2 m_e} \quad (= 2.82\ 10^{-15}\ \text{m}) \qquad (4.5)$$

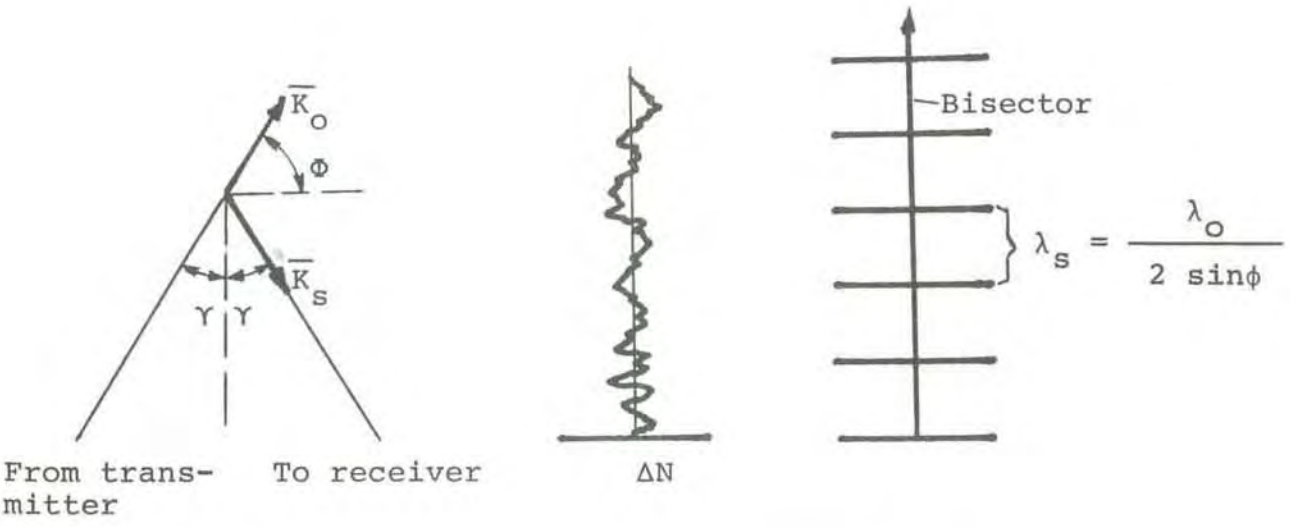

Fig. 4.1 Scatter geometry and electron density fluctuations

The total field, being the resultant of all scattered wavelets, is obtained by an integration over the scattering volume.

To find the scattered power and its distribution with frequency we may proceed to form the Autocorrelation Function of the received field:

$$\rho(\tau) = < E_s (\omega_o , t) E_s^*(\omega_o , t + \tau) > \qquad (4.6)$$

$< >$ denotes expectation value or ensemble average, $E_s^*(\omega_o, t+\tau)$ is the complex conjugate of the field taken with a time displacement τ. It may be shown (Farley, 1971) that the expression for the autocorrelation function is approximately given by:

$$< E_s(\omega_o , t) E_s^*(\omega_o , t+\tau) > = r_e^2 E_o^2 \sin^2 \xi \frac{e^{-i\omega_o \tau}}{R^2} \int_{V_s} d\bar{r} \int_{\infty} <\Delta N (\bar{r},t) \Delta N(\bar{r}+\bar{r}',t+\tau)> e^{i\bar{k}\cdot\bar{r}'} d\bar{r}' \qquad (4.7)$$

V_s is the scattering volume. ΔN is the difference between the local and the mean electron density. The inner integral describes the spatial Fourier transform of the unnormalized space and time autocorrelation function of the electron density fluctuations. By a Fourier transformation in time as well we obtain an expression for the Power Distribution in frequency:

$$< |E(\omega_o+\omega)|^2 > = r_e^2 E_o^2 V_s \sin^2 \xi (1/R^2) <|\Delta N(\bar{k},\omega)|^2> \qquad (4.8)$$

The Average Differential Cross Section is given by:

$$\sigma(\omega_o+\omega)\, d\omega = r_e^2 \sin^2 \xi <|\Delta N(\bar{k},\omega)|^2 > d\omega \qquad (4.9)$$

σ is the average power scattered through the angle ξ per unit solid angle per unit incident power per unit volume per unit frequency. For backscattering (receiver at transmitter location) $\xi = 90^o$ and we have:

$$\sigma(\omega_o+\omega) = r_e^2 <|\Delta N(\bar{k},\omega)|^2> \qquad (4.10)$$

$|\Delta N(\bar{k},\omega)|^2$ is the so-called Fluctuation Spectrum, describing how the random electron variations are distributed in frequency and spatial wave components. Several authors have derived expressions for the spectrum, using different approaches, but es-

sentially arriving at similar results. (Salpeter,1960; Dougherty & Farley, 1960; Fejer, 1961; Hagfors, 1961; Bauer, 1975; Trulsen & Bjørnå, 1977).

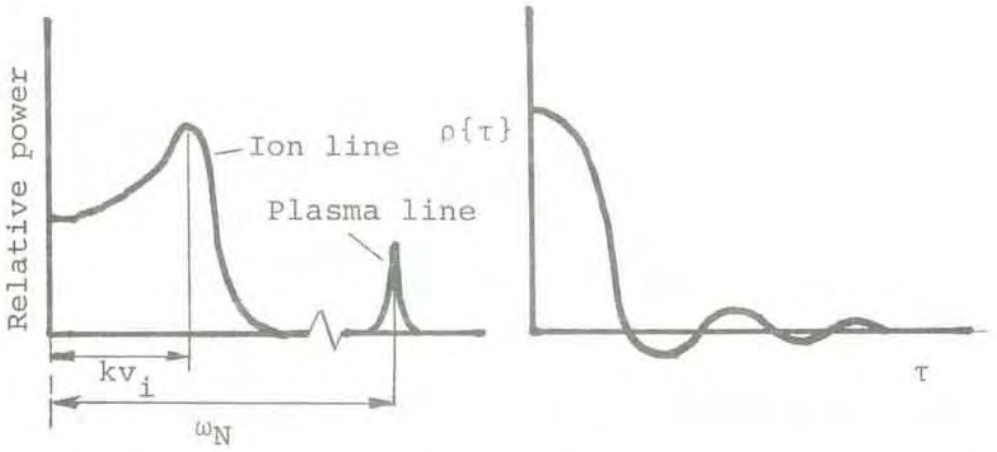

Fig. 4.2 Power spectrum and autocorrelation function

A typical autocorrelation function and a power spectrum are depicted in figure 4.2. It should be noted that since the spectrum may be derived from the correlation function, or vice versa, by a Fourier transformation, both presentations contain the same amount of information. Some kind of correlator is required for measurements of $\rho(\tau)$. The power spectrum can be observed by the use of a filter bank. The majority of existing scatter facilities seem to rely the correlator approach, but the filter bank method is also in current use (Bauer et al, 1974). We may mention that EISCAT will be equipped with a digital correlator capable of performing high speed processing of 8-bit samples of the observed field.

In discussing the characteristics of the autocorrelation function and the power spectrum there are several features to be noticed:

1. As indicated by figure 4.2 the spectrum consists of two parts: (i) the central portion of the spectrum, covering a band of some kHz, at most a few tens of kHz, on both sides

of the transmitted frequency, and (ii) narrow lines at positions displaced from the central frequency by approximately the plasma frequency (f_N) at the sampling height. The central portion is called the Ion Line, the narrow spectra labelled under (ii) above are usually termed Plasma Lines.

Due to the small amount of power contained in the plasma lines, they are likely to remain unobserved under thermal equilibrium conditions. When non-equilibrium prevails, for instance, under the influence of impinging magnetospheric particles or energetic photo-electrons, density waves, giving rise to the plasma lines, may be stimulated. At the EISCAT latitude one expects that particle fluxes of magnetospheric origin at times will dominate as the plasma line generating mechanism.

2. The two component spectrum described above corresponds to $\lambda_D << \lambda$, conditions for which the Debye length is much smaller than the exploring wavelength. This will be the case in most practical circumstances. For $\lambda_D >> \lambda$ the spectrum broadens and assumes a Gaussian shape.

3. The shape of the ion spectrum depends in a complex way on a range of parameters, such as ion composition, the ratios T_e/T_i and λ_D/λ, collision frequencies, electrical currents, plasma drifts and the direction of the geomagnetic field. For $T_e = T_i$ the shoulders in the spectrum are displaced by $\Delta f = (2/\lambda)(kT_i/m_i)^{\frac{1}{2}} = (2/\lambda)\, v_i$ from the transmitted frequency, corresponding to the Doppler frequency experienced for scatterers moving towards and away from the observer with the thermal velocity of the ion (in this formula k denotes Boltzmann's constant). The observation that the width of the spectrum is determined by the ion dynamics, despite the fact that the electrons are the actual scatterers is indicative of the Coulomb force fields which exist between the two oppositely charged species. Each ion perturbs the trajectories of the electrons within a Debye sphere. Thereby the random motion of the ions causes statistical fluctuations in the electron positions. Only when the exploring wavelength is much smaller the than the Debye length, do the electrons scatter independently. Strictly speaking it is only in this extreme case that we are entitled to talk of "incoherent" scattering. The plasma lines may be ascribed to the repulsive effects which the electrons exert upon each others.

4. The fluctuations may be described in terms of a spectrum of waves, continously distributed in direction and wavelength. The ion lines may be envisaged as caused by acoustic waves, the plasma lines by plasma electron waves. The radar acts a spectrum analyser, picking out a single component in this spectrum, the wave propagating with wave-vector along $\bar{k}$ (as defined by equation 4.4) and having a wave length satisfying the condition for constructive interference, $\lambda_s = (\lambda_D/2)(\sin \Phi)^{-1}$.

In figure 4.1 is indicated how density fluctuations along k may look like at a given time. Illustrated also is the spatial fluctuation component responsible for the scattered returns. Since the fluctuation pattern continuously changes, so will also the spatial density component considered. It will go through a continuous cycle of formation disappearance and reformation. This brings out important fact: in scatter observations the information-bearing signal has a random, or noise-like, character. Only through an integration process, involving successive repetitions of the transmission and sampling can statistically reliable data be obtained.

5. For a current free, non-moving plasma the power spectrum will be symmetric with respect to the transmitted frequency. If the plasma is moving as a whole (electrons and ions together) the spectrum retains it symmetrical shape, but is displaced by an amount $\Delta f = v_d/\lambda_s$, where v_d is the drift velocity along the bisector. A current flowing in the plasma will give rise to an asymmetric spectrum.

It may be noted that the autocorrelation function is real for drift and current free plasmas. Drifts and/or currents render the correlation function a complex quantity.

4.3 Total scattering cross section

The total scattered power (per unit solid angle per unit volume per unit incident power) is obtained by integrating 4.10 over all Doppler frequencies. Under certain conditions this may be done analytically (Farley, 1971) and the following expression is found:

$$\sigma_t = \int_{-\infty}^{\infty} \sigma(\omega+\omega_o)\,d\omega = N r_e^2 \sin^2 \xi \left[\frac{k^2\lambda_D^2}{1 + k^2\lambda_D^2} + \frac{1}{(1 + \lambda k^2\lambda_D^2)(1+T_e/T_i+k^2\lambda_D^2)} \right]$$

(4.11)

Here the first term within the bracket corresponds to the electronic or plasma-line part of the spectrum, the second term refers to the ionic part. N is the electron density. We note the following asymptotic cases:

1) $T_e = T_i$

$$\sigma_t = N r_e^2 \sin^2 \xi \left[\frac{1 + k^2 \lambda_D^2}{2 + k^2 \lambda_D^2} \right] \qquad (4.12)$$

which for $\lambda >> \lambda_D$ reduces to:

$$\sigma_t = \tfrac{1}{2} N r_e^2 \sin \xi \qquad (4.13)$$

For $\lambda << \lambda_D$ and equal temperatures the total cross section becomes:

$$\sigma_t = N r_e^2 \sin \xi \qquad (4.14)$$

2) For $T_e \neq T_i$ and $\lambda >> \lambda_D$

$$\sigma_t = N r_e^2 \sin^2 \xi \left[\frac{1}{1 + T_e/T_i} \right] \qquad (4.15)$$

4.4 Radar Equation

4.4.1 Monostatic pulsed operation

Let us briefly consider the height resolution obtained with the scatter radar in the monostatic mode. At an arbitrary time t_1, measured from the leading edge of the pulse, the scattered signal level is sampled. A part of the signal strength observed at this instance will be caused by scattering by the leading edge of the pulse at a range $R_1 = ct_1/2$. It is also clear that there will be a contribution from scattering by the trailing pulse edge at the range $R_2 = c(t_1-\tau)/2$, as well as from the range interval between R_1 and R_2. Consequently the range resolution is:

$$\Delta R = ct_1/2 - c(t_1-\tau)/2 = c\tau/2 \qquad (4.16)$$

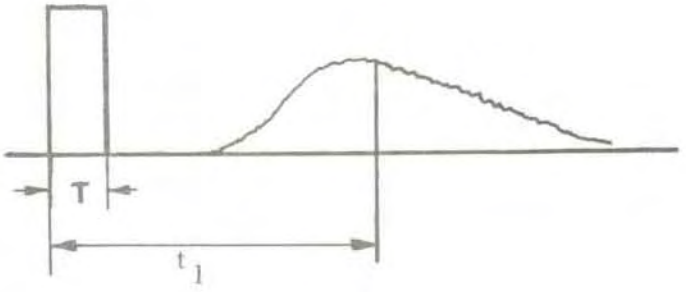

Fig 4.3 Transmitted pulse and received echo

In the geometry depicted in figure 4.4 the radar is situated at the origin of the coordinate system. We consider in the first instance scattering from the elemental volume:

$$dV = \frac{c\,\tau}{2} R^2 \sin\theta d\theta d\Phi \qquad (4.17)$$

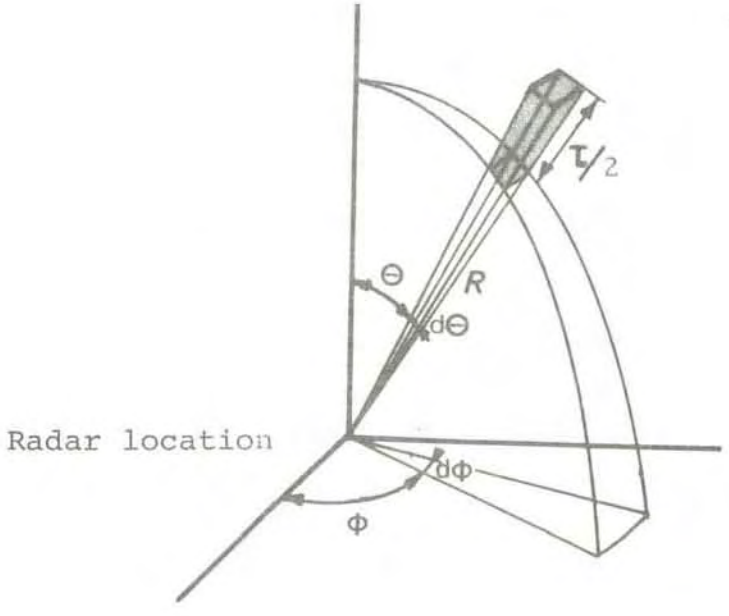

Fig. 4.4 Monostatic scatter geometry

Power incident on the scattering volume:

$$P_i = \frac{P_t L_t G(\Theta,\Phi)}{4\pi R^2} \qquad \text{(Watt m}^{-2}\text{)} \qquad (4.18)$$

where the symbols are defined as follows:
P_t - power at the transmitter output
L_t - a factor accounting for feeder losses
$G(\Theta,\Phi)$ - antenna gain

Power scattered from the elemental volume:

$$P_s = \frac{P_t G(\Theta,\Phi)}{4\pi R^2} \sigma_t dV \qquad \text{(Watt ster}^{-1}\text{)} \qquad (4.19)$$

With an effective antenna area of A_o the power received by the antenna is:

$$P_r = \frac{P_t L_t G(\Theta,\Phi)}{4\pi R^2} \sigma_t dV \frac{A_o}{R^2} \qquad (4.20)$$

A_o relates to the antenna gain in the following way:

$$A_o = \frac{G(\Theta,\Phi)\lambda^2}{4\pi} \qquad (4.21)$$

To obtain the total received power we have to integrate over all scattering volumes:

$$P_{rt} = \frac{P_t L_t c\tau\lambda^2 \sigma_t}{2(4\pi)^2 R^2} \iint G(\Theta,\Phi)^2 \sin\Theta d\Theta d\Phi \qquad (4.22)$$

Assuming an axisymmetric antenna and inserting expression (4.15) for σ_t we obtain:

$$P_{rt} = \left[\frac{P_t L_t c\tau\lambda^2 r_e^2}{16\pi} \int G(\Theta)^2 \sin\Theta d\Theta \right] \frac{N}{R^2(1+T_e/T_i)} \qquad (4.23)$$

The value of the bracketed expression may be found by careful measurements of the radar parameters or by alternative means for determining N. It should be noted that the average received power is given by the zero lag autocorrelation function (expression 4.6).

4.4.2 Bistatic Operation

Whereas in monostatic operation an arbitrary height may be sampled simply by setting the range gate at the appropriate time, in a bistatic system the height will be determined by the geometry of the antenna beams as indicated in figure 4.5.

Repositioning of one or both antennas is required to effect a change in the sampled height or in the coordinates of the scattering volume.

The radar equation for the bistatic case is obtained by redefining some parameters in equation (4.20). The power received from an elemental volume is given by:

$$P_r = \frac{P_t L_t G(\Theta)}{4\pi R_t^2} \sigma_t dV \frac{A_r}{R_r^2} \qquad (4.24)$$

Here R_t and R_r denote the distances of the scattering volume from the transmitter and receiver respectively, and A_r the effective area of the receiving antenna. Again, the expression for the total received power is obtained by an integration over the scattering volume.

We shall not here go into details of bistatic scattering, but refer to reports of Evans (1967) and Murdin (1978). Especially the latter reference may be valuable, as it specifically pertains to the EISCAT facility.

It is readily apparent that the effective scattering volume will vary with time as a pulse passes through the space intersected by the two beams. For long pulses the volume may extend outside the receiver antenna beam. In this case the volume is said to be beam width limited. For shorter pulses the effective volume may occupy only a part of the intersection space. This latter case is referred to as being pulse length limited.

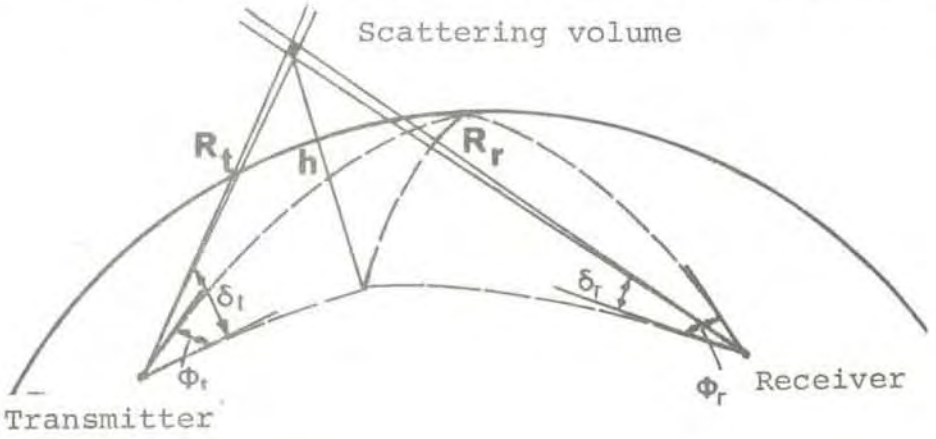

Fig. 4.5 Bistatic scattering

5 NOISE

5.1 Some basic concepts and definitions

The random motion of the electrons in any conductor at a temperature other than absolute zero gives rise to a noise voltage whose mean-square value is:

$$\overline{e_n^2} = 4\ kRTB \qquad (5.1)$$

where k is Boltzman constant, T the absolute temperature in degrees Kelvin, R the resistance of the conductor and B the bandwidth of the noise. Noise generated in the conductor may be represented as a noise free resistance in series with a noise voltage source with the mean square value given by (5.1) From network theory we know that the maximum power which may be transferred from the generator to a load occurs under "matched" conditions, with the load equal to the complex conjugate of the source impedance. This gives for the maximum available noise power:

$$N_{av} = kTB \qquad (5.2)$$

Noise of this nature is called Thermal Noise, to signify its dependence upon temperature. We note that the noise power is independent of the value of the resistance. Throughout the microwave region the generated spectrum remains constant, constituting what is termed White Noise.

All practical receivers generate noise to some extent. A measure of the noise of the receiver compared with the noise of an ideal receiver (with no internal noise sources) constitutes the Noise Factor:

$$F = \frac{\text{total noise power at the output}}{\text{output noise power due to the source}} = \frac{N}{kT_oBG} \qquad (5.3)$$

By convention $T_o = 290^oK$, close to ordinary room temperature; G is the power gain. If the signal power entering the receiver is P, we can write:

$$F = \frac{P/kT_oB}{GP/N} \qquad (5.4)$$

Provided the input source resistance temperature is 290^o, the noise factor is equal to the signal-to-noise ratio at the input of the receiver (amplifier) divided by that at the output.

We note that the noise figure has a minimum value of 1, or zero, measured in decibels, corresponding to an ideal network with no internal noise sources.

The total output noise power consists of two terms:

$$N = kT_oBG + \Delta N \tag{5.5}$$

where ΔN accounts for the noise created within the network. For low-noise amplifiers the noise performance is frequently expressed by an effective noise temperature, T, defined as that temperature at the input of the network which yields the actual noise ΔN at the output.
We obtain the following relation:

$$F = \frac{kT_oBG + kTBG}{kT_oBG} = \frac{T_o + T}{T_o} \tag{5.6}$$

$$T = T_o(F-1) \tag{5.7}$$

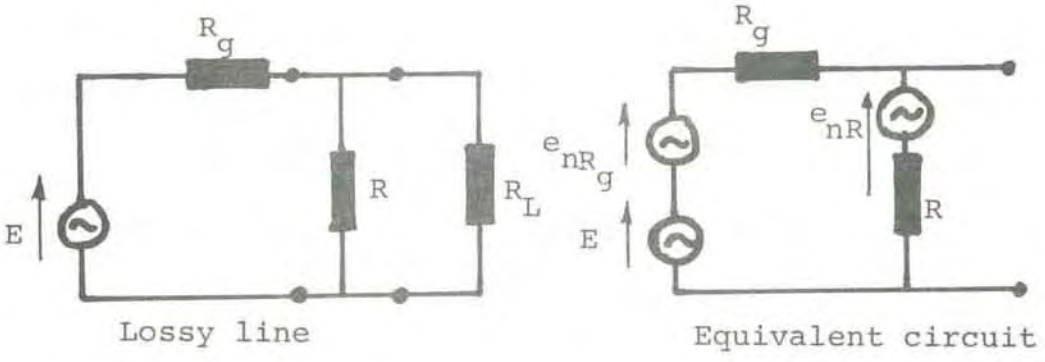

Figure 5.1 Illustration of lossy line with equivalent circuit containing noise generators

Any losses in transmission lines, duplexers and antennas result in noise. In the four terminal network in figure 5.1 the transmission line is represented by a resistor between the source and the load of the system. The source could, for instance, be an antenna and the load a low-noise amplifier. The analysis is, however, quite general. In the illustration the noise generated by

R_g and R are represented by equivalent voltage sources inserted in the respective branches. We assume that R is at temperature T and that the source has the standard temperature T. We also assume that the noise sources are uncorrelated.

The available power gain (actually a loss), defined as the available output power divided by the available input power, is:

$$G = \frac{R}{R_g + R} = \frac{1}{L} \tag{5.8}$$

Our analysis gives for the output noise:

$$N = \frac{RT_o + R_g T}{R + R_g} kB \tag{5.9}$$

By combining (5.3), (5.8) and (5.9) we obtain:

$$F = 1 + (L - 1)\frac{T}{T_o} \tag{5.10}$$

Correspondingly the temperature to the input of the transmission line is:

$$T_i = T(L - 1) \tag{5.11}$$

Let us next briefly consider the noise behaviour of a chain of cascaded stages. We assume that the stages are matched at the output, implying that the stage gains are equal to the available gains. We may write for the noise factor:

$$F = \frac{N}{kT_o BG_1 G_2 \ldots G_n} = 1 + \frac{N_{int}}{kT_o BG_1 G_2 \ldots G_n} \tag{5.12}$$

where G_1, G_2, etc. are the stage gains.

The total output noise will have contributions from each stage:

$$N_{int} = N_1 + N_2 \ldots\ldots N_n$$
$$= kBG_1 G_2 \ldots G_n \left(T_1 + \frac{T_2}{G_1} + \ldots + \frac{T_n}{G_1 G_2 - G_{n-1}}\right) \tag{5.13}$$

Denoting the effective system temperature T_e we have:

$$kBT_e G_1 G_2 \ldots G_n = N_{int} \tag{5.14}$$

Combining the last two expressions:

$$T_e = T_1 + \frac{T_2}{G_1} + \frac{T_3}{G_1 G_2} + \ldots + \frac{T_n}{G_1 G_2 \ldots G_{n-1}} \qquad (5.15)$$

Furthermore we find for the system's noise factor:

$$F_e = F_1 + \frac{F_2 - 1}{G_1} + \frac{F_3 - 1}{G_1 G_2} + \ldots + \frac{F_n - 1}{G_1 G_2 \ldots G_{n-1}} \qquad (5.16)$$

(5.15) and (5.16) bring out an important feature: if the gains of the stages in a cascaded network, in particular the gain of the first stage, are high, the overall noise performance of the system essentially depends upon the noise contribution of the first stage. This is the reason why there are often stringent requirements on the quality of the preamplifiers in low-noise applications. The amplifiers should be located as close as possible to the source.

5.2 Antenna noise

The power available at the output terminals of an antenna will be proportional to the energy flux density, S_m, of the source being measured.

$$p = A(\theta,\Phi) S_m \quad (\mathrm{WHz}^{-1}) \qquad (5.17)$$

where the subscript m indicates that the polarization is matched to that of the antenna. The proportionality constant, $A(\theta,\Phi)$, is the Effective Area of the antenna, a quantity which depends upon the direction of the incoming radiation. $A(\theta,\Phi)$ is generally less, at most equal to, the geometrical antenna area and describes how effective the antenna is in making the extracted power available at the antenna output.

In practice radiation is arriving from all directions. Contributions from different parts of space are uncorrelated. As a result the total power is composed of components from different locations in space adding linearly.

Radio Brightness is defined as the flux density per unit solid angle of sky as a function of direction. For matched polarization we may write:

$$B_m(\Theta,\Phi) = \Delta S_m/\Delta\Omega \qquad (5.18)$$

where $\Delta\Omega$ is the elemental solid angle.
By combining expressions (5.17) and (5.18), and integrating over the whole sky, we obtain the total power at the antenna output:

$$p_t = \int B_m(\Theta,\Phi)\ A(\Theta,\Phi)d\Omega \quad (WHz^{-1}) \qquad (5.19)$$

By equating the received power, p_t, to the thermal noise from a resistor of temperature T_a:

$$p_t = kT_a \qquad (5.20)$$

It is the temperature of this fictitious resistor that is called Antenna Temperature. It should be noted that as defined here, the antenna temperature is an average quantity depending upon the radiation arriving from all directions, including contributions coming in through the side and back lobes. Should the antenna be positioned in such a way that the side lobes intersect the ground, a notable contribution may be due to the noise from the "hot" ground. It should be noted that T_a indicates a power level and need have no relation to any real temperature.

5.3 Galactic and atmospheric noise

The sources of cosmic radio noise form a broad diffuse band concentrated along the galactic equator and toward the galactic centre. Superposed on this background are numerous discrete "radio stars", of which those in the constellations of Cassiopeia and Cygnus may be best known. As a result of the nonuniformity of the source distribution antenna temperatures generally vary with pointing direction. Higher temperatures are observed for low elevation angles than for antennas pointing vertically. At frequencies above 1 GHz noise generated by the atmosphere dominates over the galactic component.

Another important radio noise source is the sun. At 1 GHz the flux density from Cassiopeia amounts to about $2.6\ 10^{-23} Wm^{-2}Hz^{-1}$. At the same frequency the sun contributes with about $3.6\ 10^{-21} Wm^{-2}Hz^{-1}$. It should be noted, though, that the solar radiation may increase

by several orders of magnitude during solar storms.

Figure 5.2 shows how the galactic background and the hot spot noise, expressed in terms of averaged antenna temperatures, varies with frequency.

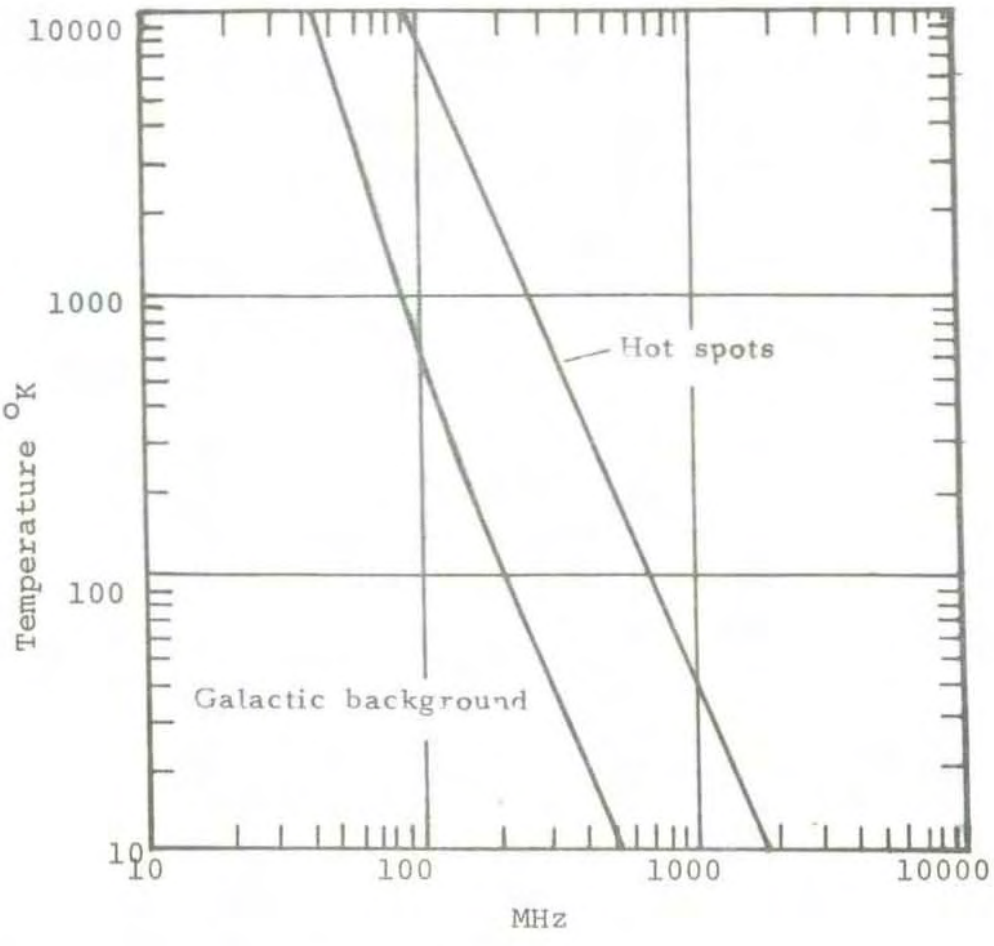

Fig. 5.2 Galactic noise

References chapter 4 and 5

Bauer, P, P Waldteufel and C Vialle - Radio Sci 9, 77(1974)

Bauer, P - Phil Trans Roy Soc (London) A 280, 167(1975)

Dougherty, J P and D T Farley - Proc Roy Soc (London) A 259, 79(1960)

Evans, J V Y T Lo - Aeronomy Report No. 23, University of Illinois (1967)

Farley, D T - Methods of Experimental Physics 9B, Eds R H Lovberg and H R Griem, Academic Press (1971)

Fejer, J A - Can J Phys 39, 716(1961)

Hagfors, T - J Geophys Res 66, 1699(1961)

Murden, J - SNR for the EISCAT UHF System KGI Report No 78:1(1978)

Salpeter, E E - Phys Rev 120, 1528(1960)

Trulsen J and N Björnå - Radar Probing of the Auroral Plasma, Ed A Brekke, Universitetsforlaget (1977)

6 WAVE POLARIZATION

6.1 Introduction

The term wave polarization refers to the behaviour of the electric field vector in electromagnetic waves. In the general case polarization is elliptical, i.e. for a given location the locus of the tip of the electric field vector describes an ellipse. Linear polarization results when the ellipse degenerates into a line, with the length of one of the axes approaching zero.

The EISCAT facility will be provided with several polarization options. In both the UHF- and the VHF-system can one freely select between right- and left-hand circular polarization. In addition, in the UHF-system, linear polarization with the electric field vector pointing in an arbitrary direction may be realized. The possibility for linear polarization is also inherent in the VHF-facility, though not with the same flexibility as built into the UHF-feed for freely selecting the polarization plane.

6.2 Definitions and basic relations

Two quantities varying harmonically with time and differing by $\pi/2$ (90°) in phase are referred to as being in time or phase quadrature. In complex representation a 90° phase factor appear as $e^{j\,\pi/2} = j$. Two vector quantities $\bar{a}$ and $j\bar{b}$ are consequently in phase quadrature.

Orthogonal vectors are sometimes said to be in space quadrature. If $\bar{a}$ and $\bar{b}$ referred to above satisfy the relation:

$$\bar{a} \cdot \bar{b} = 0 \qquad (6.1)$$

the vectors $\bar{a}$ and $j\bar{b}$ are both in space and time quadrature.

Providing for complex vector notation two vectors $\bar{v}$ and $\vec{u}$ are defined to be orthogonal if:

$$\bar{v} \cdot \vec{u}^{*} = 0 \qquad (6.2)$$

In the framework of harmonic time variations a complex vector represents an ellipse. The general definition implies that two vectors are orthogonal if and only if the ellipses which represent them have the same axial ratio, opposite sense of rotation, and major axes perpendicular.

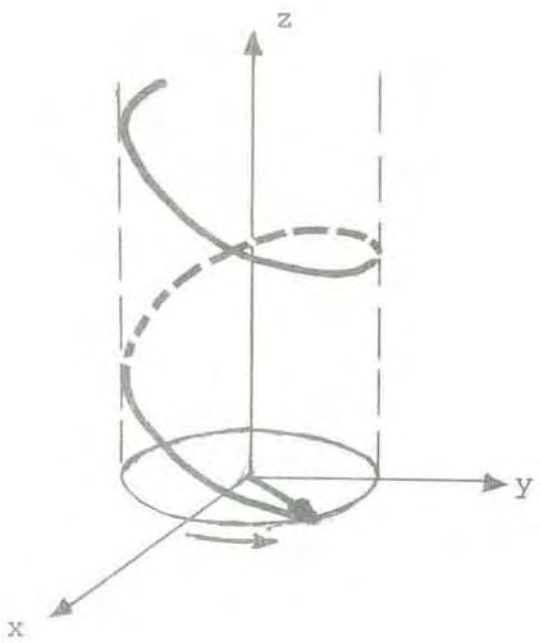

Figure 6.1 Right-handed circularly polarized wave travelling along z-axis

The notations used in the past for right- and left-hand sense of rotation appear to have caused much confusion.
Figure 6.1 represents a circular wave propagating along the z-axis. Viewed from the origin the field vector rotates counterclockwise along the z-axis. However, for any fixed location the rotation is clockwise with respect to time. In keeping with modern usage this wave is described as having right-hand polarization. We may emphasize, though, that right-hand polarization with respect to time implies left-hand rotation with respect to space, and vice versa. In complex notation wave polarization is defined as the ratio of the y- and x-field components

$$\rho = \frac{E_y}{E_x} \qquad (6.3)$$

6.3 Theory

Let us consider a plane wave travelling along the z-axis with the components:

$$E_x = E_1 \cos(\omega t - kz) \qquad (6.4)$$

$$E_y = E_2 \cos(\omega t - kz + \delta) \qquad (6.5)$$

E_1 and E_2 are (real) constants, $k = 2\pi/\lambda$ and δ is the phase difference of E_y and E_x. The total field may be written:

$$\bar{E} = E_x \hat{i}_x + E_y \hat{i}_y \qquad (6.6)$$

Where $\hat{i}_x$ and $\hat{i}_y$ denote unit vectors along the x- and y-axes. Expanding (6.5) for $z = 0$:

$$E_y = E_2[\cos \omega t \cos \delta - \sin \omega t \sin \delta] \qquad (6.7)$$

From (6.4)

$$\cos \omega t = \frac{E_x}{E_1} \qquad (6.8)$$

$$\sin \omega t = \sqrt{1 - \left(\frac{E_x}{E_1}\right)^2} \qquad (6.9)$$

By introducing (6.8) and (6.9) in (6.7) time is eliminated:

$$E_y = E_2 \left[\frac{E_x}{E_1} \cos \delta - \sqrt{1 - \left(\frac{E_x}{E_1}\right)^2} \sin \delta\right] \qquad (6.10)$$

which gives:

$$\left(\frac{E_x}{E_1}\right)^2 - 2\frac{E_x E_y}{E_1 E_2} \cos \delta + \left(\frac{E_y}{E_2}\right)^2 = \sin^2 \delta \qquad (6.11)$$

Equation (6.11) represents an ellipse in its most general form, the axes of the ellipse not coinciding with the x- and y-axes.

The field components E_x and E_y may be expressed in terms of the components E_x' and E_y' in a coordinate system rotated through an arbitrary angle α

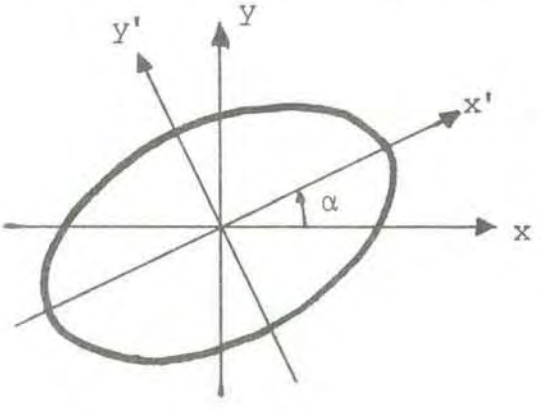

Figure 6.2 Elliptical polarization

$$E_x = E_x' \cos\alpha - E_y' \sin\alpha \qquad (6.12)$$

$$E_y = E_x' \sin\alpha + E_y' \cos\alpha \qquad (6.13)$$

In general the new ellipse contains a product term $CE_x'E_y'$. For $\alpha=\gamma$ the x'- and y'-axes coincide with the axes of the ellipse and the product term disappears (C=0). Noting this property we obtain an expression for γ:

$$\operatorname{tg} 2\gamma = 2\cos\delta \frac{E_1E_2}{E_1^2-E_2^2} \qquad (6.14)$$

Introducing for the ratio E_2/E_1:

$$R = \frac{E_2}{E_1} \qquad (6.15)$$

we obtain:

$$\operatorname{tg} 2\gamma = 2\cos\delta \frac{R}{1-R^2} \qquad (6.16)$$

with $\alpha = \gamma$ the ellipse equation becomes:

$$\frac{E_x'^2}{(\frac{A}{2})^2} + \frac{E_y'^2}{(\frac{B}{2})^2} = 1 \qquad (6.17)$$

where A and B are the lenghts of the major and minor axes of the ellipse.

By substituting (6.12) and (16.13) in (6.11) we find:

$$(\frac{B}{A})^2 = \frac{R^2\cos^2\gamma + \sin^2\gamma - R \sin 2\gamma \cos\delta}{R^2\sin^2\gamma + \cos^2\gamma + R \sin 2\gamma \cos\delta} \qquad (6.18)$$

Discussion:

1) Circular polarization

$A = B,\ R = 1, \delta = \pm \pi/2$

From (6.3) and (6.4) , with z = o:

$$E_x = E_o \cos \omega t \qquad (6.19)$$

$$E_y = E_o \cos(\omega t \pm \pi/2) = \mp E_o \sin \omega t \qquad (6.20)$$

Figure 6.3 illustrates the polarization behaviour for $\delta = +\pi/2$ and $\delta = -\pi/2$

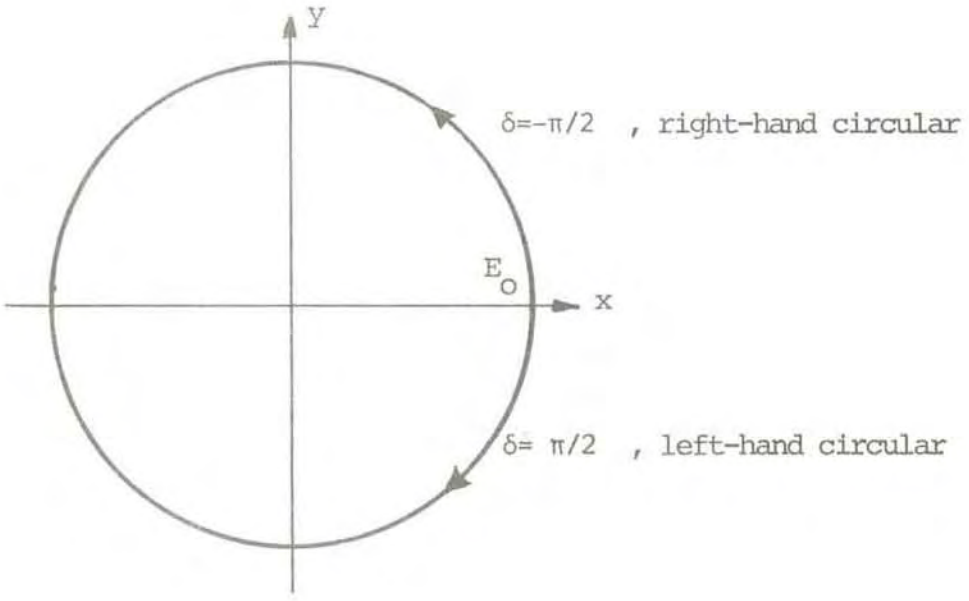

Figure 6.3 Dependence of sense of rotation upon phase

In complex description we have:

$$E_x = E_o e^{j\omega t} \qquad (6.21)$$

$$E_y = \pm j E_o e^{j\omega t} \qquad (6.22)$$

and for the polarization:

$$\rho = \pm j \qquad (6.23)$$

$\rho = j$ correponds to left-hand sense of rotation. $\rho = -j$ represents right-hand rotation.

2) Elliptical polarization

As already described in the previous sections this most general polarization may be established by an interaction of two orthogonal linearly polarized fields. By an examination of (6.17) we are led to conclude that the two field components establish an elliptically polarized wave if either:

a) the two fields are of equal amplitudes but with phases appropriately chosen or

b) the two field components are in phase quadrature with appropriately chosen amplitudes

We may note that an elliptical waveform may also be produced by superimposing two oppositely handed circular fields.

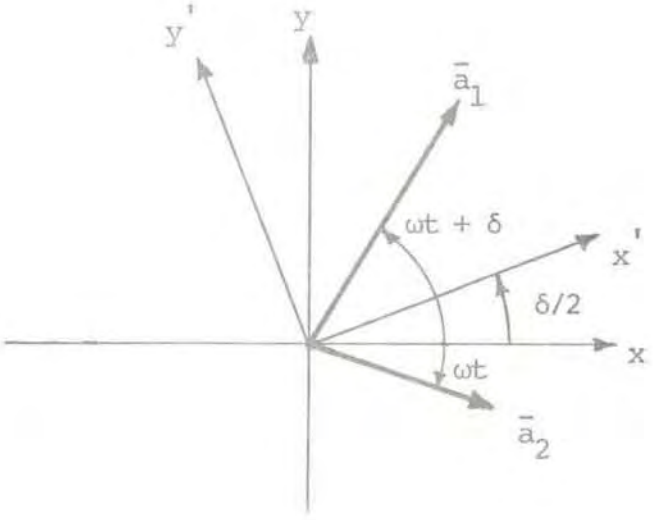

Figure 6.4 Coordinate system transformation

In figure 6.4 are depicted two rotating vectors $\bar{a}_1$ and $\bar{a}_2$, $\bar{a}_1$ being right-handed, $\bar{a}_2$ rotating with the left-hand sense. The phase difference of the two components is δ. Let us introduce a new coordinate system with the x'-axis as indicated in the figure. By inspection of the figure:

$$E_x' = (a_1 + a_2)\cos(\omega t + \delta/2) \qquad (6.24)$$

$$E_y' = (a_1 - a_2)\sin(\omega t + \delta/2) \qquad (6.25)$$

$$\frac{E_x'^2}{(a_1 + a_2)^2} + \frac{E_y'^2}{(a_1 - a_2)^2} = 1 \qquad (6.26)$$

Equation (6.26) describes an ellipse with half axes a_1+a_2 and a_1-a_2. We may digress here to present a more general description, again reverting to complex vector notation. As referred to in section 6.2 a uniform elliptically polarized plane wave may be represented in the form

$$\bar{E}(t) = \vec{\varepsilon}\, e^{j(\omega t - kz)} \qquad (6.27)$$

where $\bar{\varepsilon} = \bar{E}_r + j\bar{E}_i$ and $\bar{E}_r$ and $\bar{E}_i$ are real vectors perpendicular to the z-axis and independent of position and time (not necessarily in space quadrature). For a demonstration of this fact see Kales (1951).

If $\bar{u}$ and $\bar{v}$ are an arbitrary pair of complex, orthogonal unit vectors in the plane of the complex vector $\bar{E}$, then $\bar{E}$ may be represented in the form

$$\bar{E} = (\vec{E} \cdot \bar{u}^*)\vec{u} + (\bar{E} \cdot \bar{v}^*)\vec{v} \qquad (6.28)$$

$$= \varepsilon_u \vec{u} + \varepsilon_v \vec{v} \qquad (6.29)$$

To check the validity of (6.28) form the scalar product

$$\bar{E} \cdot \bar{u}^* = (\bar{E} \cdot \bar{u}^*)\vec{u} \cdot \vec{u}^* + (\bar{E} \cdot \bar{v}^*)\vec{v} \cdot \vec{u}^* \qquad (6.30)$$

The last term disappears since $\bar{u}$ and $\bar{v}$ are orthogonal. $\vec{u} \cdot \vec{u}^* = 1$.

From the orthogonality of $\vec{u}$ and $\vec{v}$ we find

$$|\vec{E}|^2 = \bar{E} \cdot \bar{E}^* = |\varepsilon_u|^2 + |\varepsilon_v|^2 \qquad (6.31)$$

It may be concluded from equation (6.29) that a given elliptically polarized field may be resolved into two orthogonal elliptically polarized fields in an infinite number of ways. Equation (6.31) states that the power density of the elliptical wave is composed of the power densities of any two orthogonal elliptically polarized field components.

3) Linear polarization

For $\delta=0$ equations (6.4) and (6.5) represent a line in the xy-plane

whose slope is

$$\operatorname{tg} \gamma = \frac{E_2}{E_1} \qquad (6.32)$$

We may note that linear polarization may also be realized by superimposing two circular fields of equal amplitudes. This is easily seen by inspecting equations (6.24) and (6.25). If $a_1=a_2$ the orientation of the resultant field remains fixed along the x'-axis.

6.4 Antenna polarization matching

We will not delve into a detailed treatment of the antenna matching problem. Those who are interested may consult available literature (f.inst. Sichak & Milazzo, 1948; Kraus, 1966).

Matching of a receiver antenna to an incoming wave is the condition for maximum power transfer. For matching to occur the antenna must have the same polarization as the impinging wave. By antenna polarization is meant the polarization of the wave produced by the antenna used for transmission.

A circularly polarized antenna will be blind to waves arriving with the opposite polarization. This means that the antenna, configured to operate for one sense of rotation only, will fail to detect its image, interpreted as the wave returned to the antenna upon reflection. Upon reflection a right-handed wave is turned into a wave having left-hand rotation. To receive this field the antenna must be activated to operate in the polarization mode orthogonal to that transmitted.

6.5 Polarization in multistatic operation

6.5.1 Linearly polarized wave field

From (4.7) and (4.24) it will be known that the scattered power is proportional to $\sin^2\xi$, where ξ is the angle between the electrical field vector of the wave impinging upon the scatter volume and the direction to the observer. Further the received power depends upon $1/(R_t R_r)^2$, where R_t and R_r signify the distances from the scatter centre to the transmitter and receiver respectively.

For <u>one</u> remote station the optimal vector orientation would be normal to the plane through the transmitter beam and the remote location, provided Faraday rotation is negligible (see section 6.6). With <u>two</u> remote stations, as we have in the EISCAT facility, a compromise must be

sought. It has been suggested (Westerlund, 1979) that a sensible arrangement would be to adjust the polarization settings of the transmitter and receiver antennas so as to optimize the product of the scattered powers received at the two remote sites. An example of relative powers received at Kiruna and Sodankylä, using this optimalization procedure, is shown in figure 6.5.

Figure 6.5 Relative powers received at Kiruna and Sodankylä when the polarizations are chosen to maximize the products of the powers received at the two stations. The computations refer to a height of 100 km (Murdin 1979)

In practical terms the indicated operational scheme would necessitate, for each station, sets of tabled values for the polarization settings as function of the positions of the scatter volumes.

6.5.2 Circular polarization

Let us consider the geometry illustrated in figure 6.6.

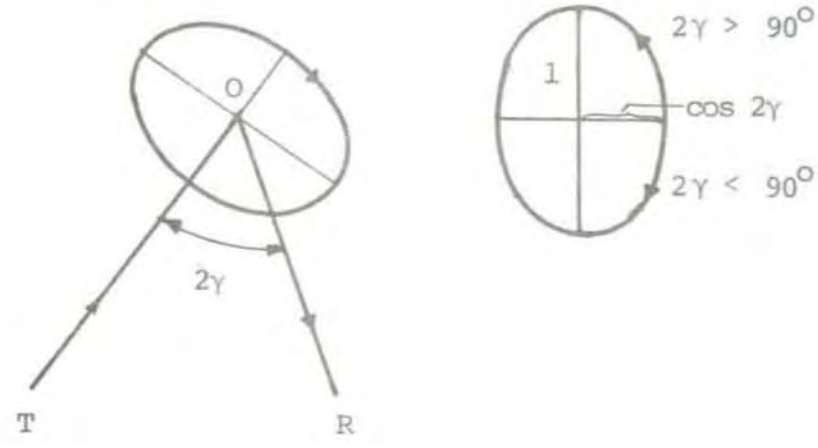

Figure 6.6 Polarization in bistatic scattering

A circularly polarized wave impinges on the scatter volume at O. Viewed from the receiver at R the circle described by the locus of the field vector at the scattering location O appears to be an ellipse, the major axis being along the normal to the plane through the two antenna beams. The length of the minor axes is found to be cos 2γ.

According to equation (6.26) the elliptical field observed in the direction of R can be regarded as composed of circulary polarized waves with amplitudes a_1 and a_2:

$$a_1 + a_2 = 1 \qquad (6.33)$$

$$a_1 - a_2 = \cos 2\gamma \qquad (6.34)$$

from which we derive:

$$a_1 = \tfrac{1}{2} (1 + \cos 2\gamma) \qquad (6.35)$$

$$a_2 = \tfrac{1}{2}\,(1 - \cos 2\gamma) \qquad (6.36)$$

The total power of the elliptical field transmitted in the direction of R relative to that scattered for optimal linear polarization:

$$|E_t|^2 = a_1^2 + a_2^2 = \tfrac{1}{2}\,(1 + \cos^2 2\gamma) \qquad (6.37)$$

If the receiver antenna is polarized to detect the dominating circular mode, the received power may be written:

$$|E_r|^2 = \frac{1}{4}\,(1 + |\cos 2\gamma|)^2 \qquad (6.38)$$

The fraction of the available power which is detected:

$$R = \frac{|E_r|^2}{|E_t|^2} = \frac{(1 + |\cos 2\gamma|\,)^2}{2(1 + \cos^2 2\gamma)}$$

$$= \tfrac{1}{2}\,\left(1 + \frac{2|\cos 2\gamma|}{1 + \cos^2 2\gamma}\right) \qquad (6.39)$$

We note the following cases:

(i) $2\gamma = 90^\circ \qquad R = 0.5$

The incoming wavefield at R appears to be linearly polarized, corresponding to equally strong circularly polarized waves, half of the power being carried by the detected wave.

(ii) $2\gamma = \ \ 0^\circ \qquad R = 1$

This approximation applies for the case when the distance between transmitter and receiver is small compared with the distance to the scattering volume.

It should be noted (indicated in figure 6.6) that the sense of rotation of the field vector describing the ellipse observable at R changes for $2\gamma = 90^\circ$. This has the implication that if one wishes to continue receiving the dominating circular mode, the hand of rotation of the receiver antenna polarization should be changed whenever a change of the scatter volume coordinates makes the angle 2γ to go through 90°.

In figure 6.7, a and b, and 6.8 we show the power ratios 6.37 to 6.39 computed for two and three different height levels.

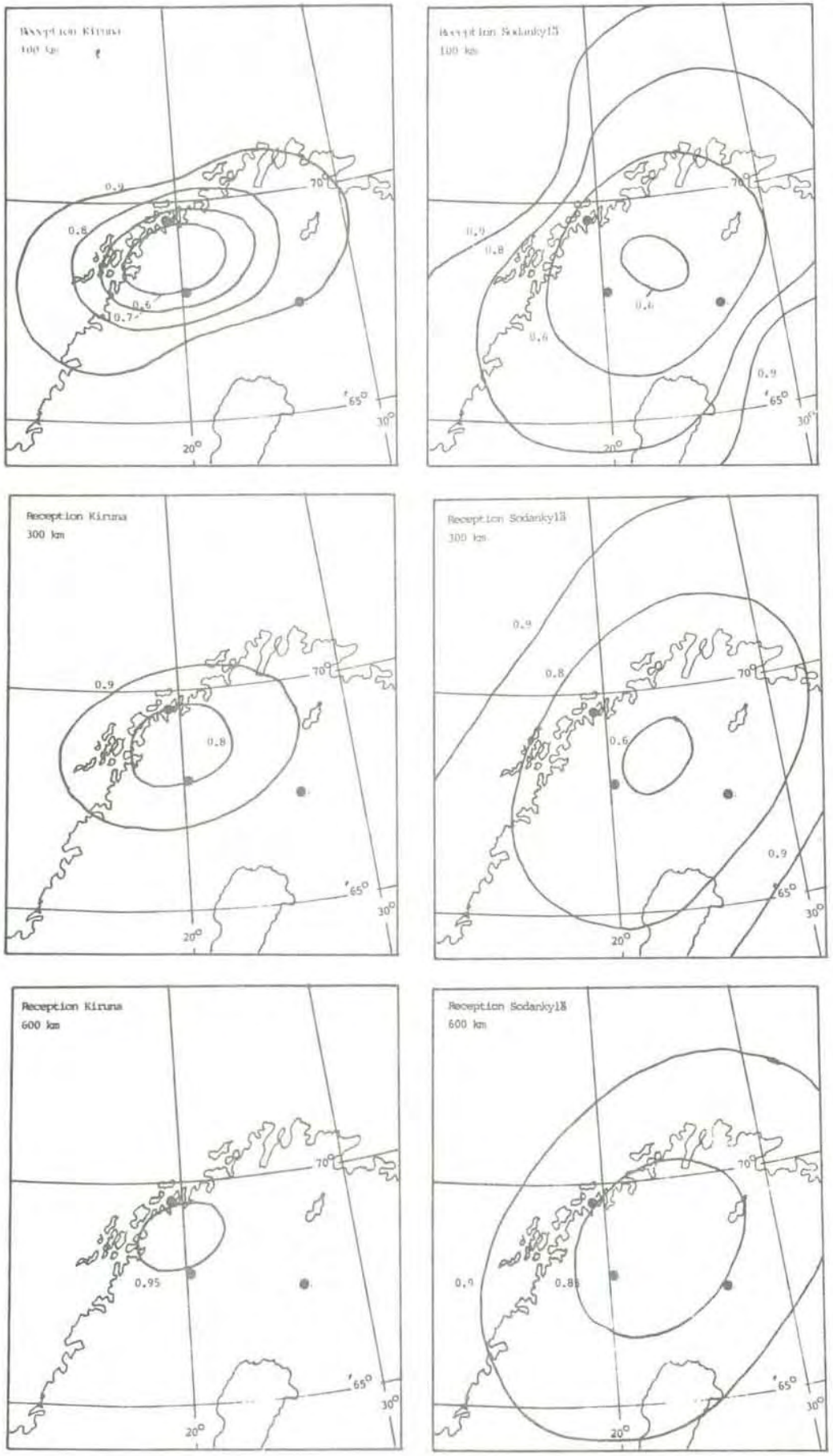

Figure 6.7 a Ratio of total power of elliptical field scattered in the direction of R and the power scattered in the same direction for optimal linear polarization (expression 6.37).

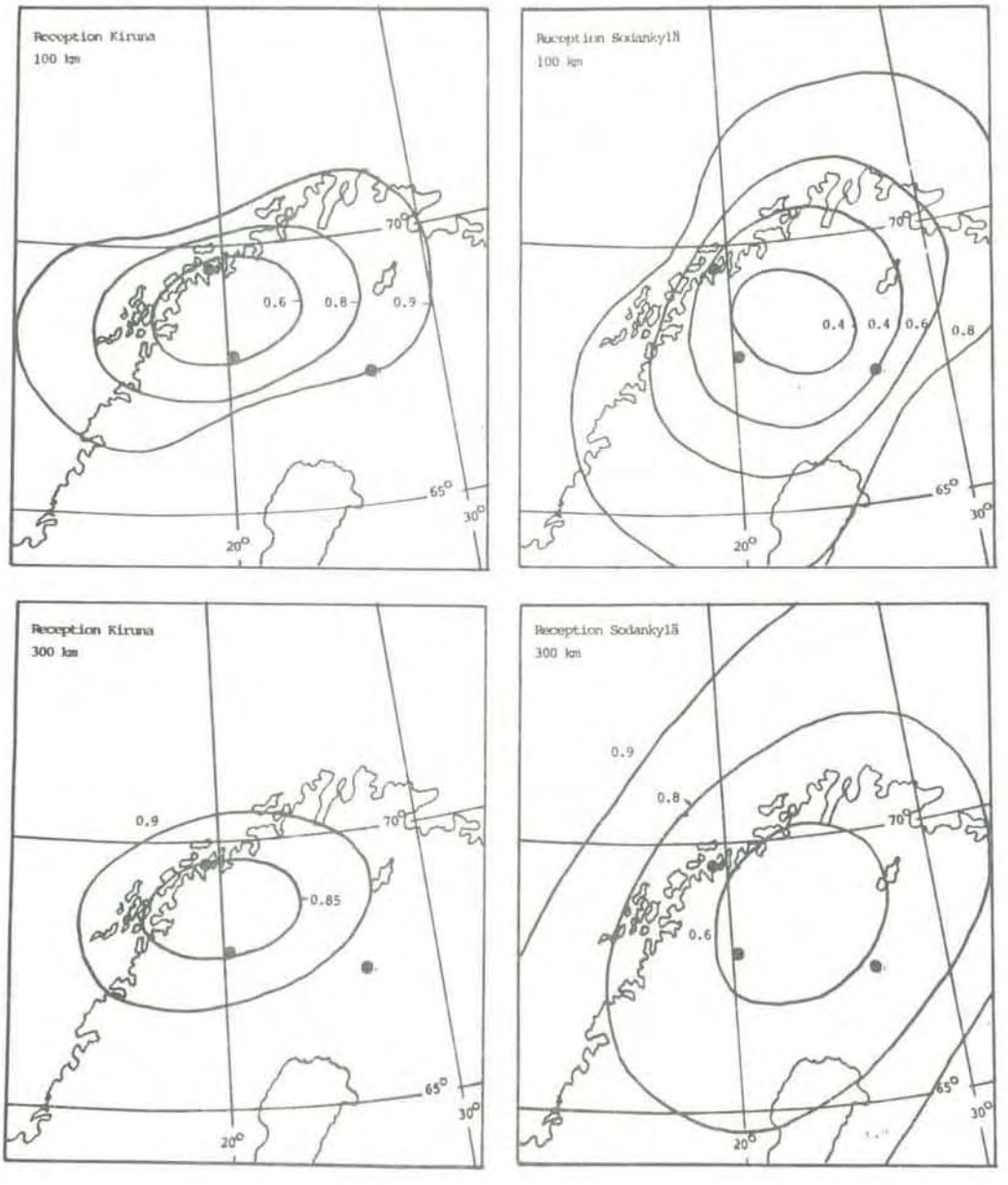

figure 6.7 b Power of dominating circular mode relative to power scattered for optimal linear polarization (expression 6.38).

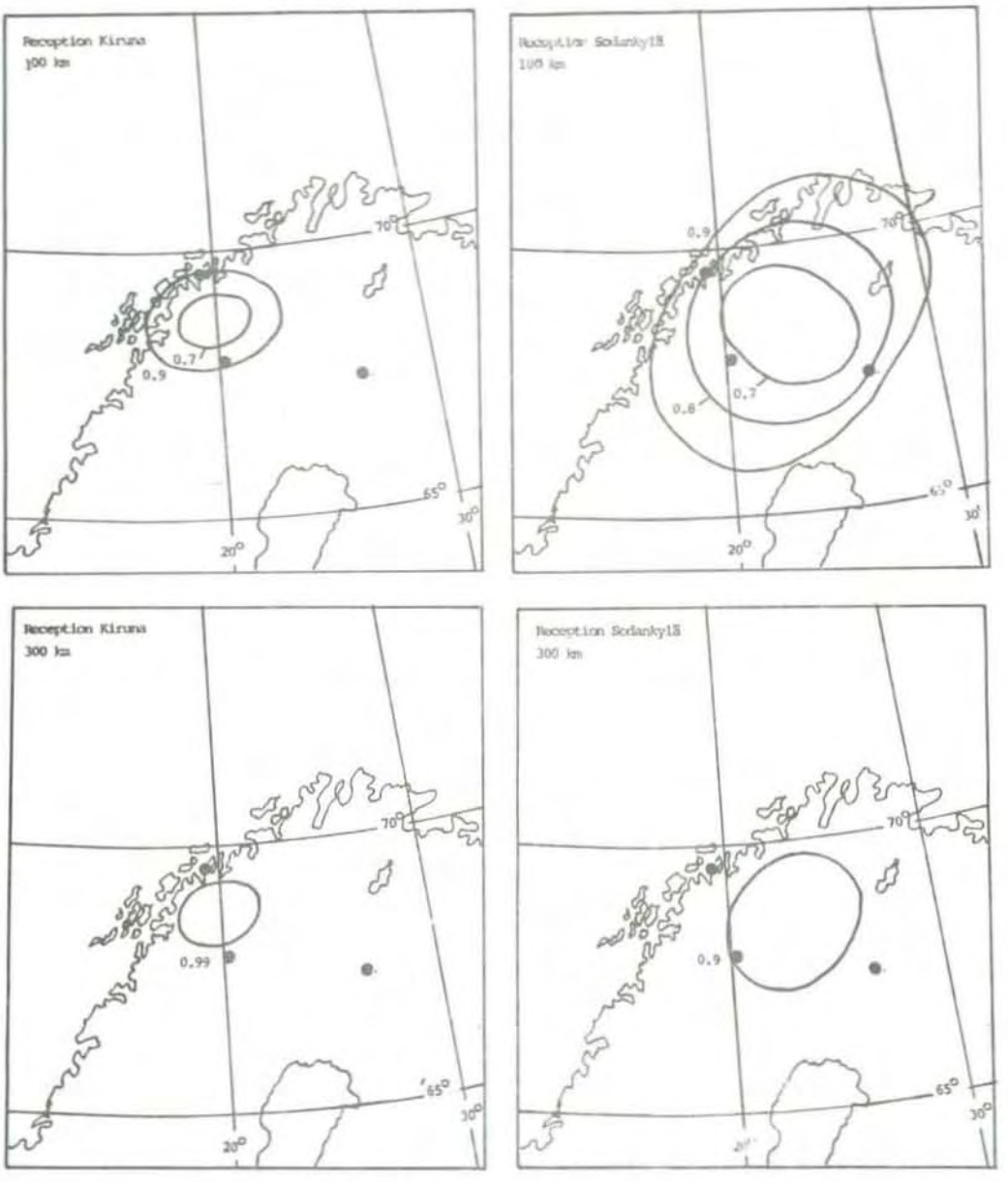

Figure 6.8 Fraction of total scattered power contained in the dominating circular mode (expression 6.39).

6.6 Faraday rotation

As indicated in section 6.3 an elliptically (or linearly) polarized wave can be regarded as being composed of a righthanded and a left-handed wave. Due to the presence of the earth's magnetic field the ionosphere is an anisotropic medium, offering different propagation conditions for the two oppositely polarized wave components. The two waves will generally travel with unequal velocities and be subject to different damping. As a consequence of this the direction of the resultant field vector, being everywhere the composite of the two component vectors, will change along the propagation path. Generally the amount of rotation depends upon the integrated electron density along the path and the angle, ϕ, between the wave vector and the geomagnetic field.

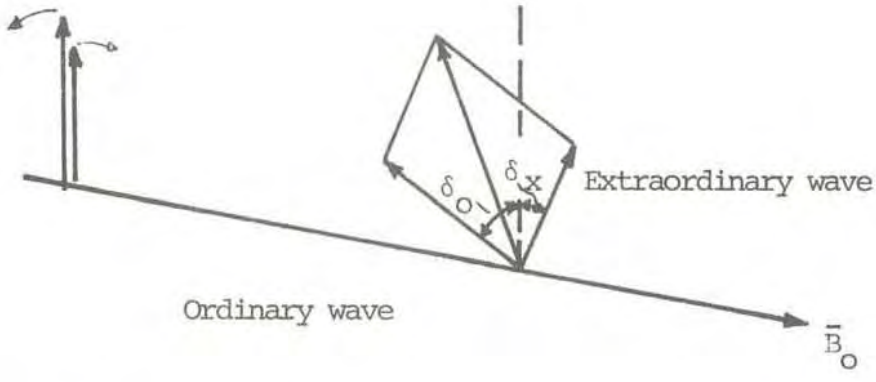

Figure 6.9 Illustration of Faraday effect for waves propagating along the magnetic field B_o.

For the longitudinal case (which apply for the EISCAT radar frequencies as long as ϕ is not close to 90^o) the Faraday rotation may be expressed as:

$$\Theta = 2.365 \cdot 10^4 f^{-2} \int_o^s \cos\phi \, BN ds \quad \text{(radians)} \qquad (6.40)$$

where N_e = electron density
B = strength of geomagnetic field
f = frequency

The integrated total columnar electron content of the ionosphere is known to vary with season and state of disturbance. Normally the integrated density (vertical direction) is between 10^{16} and 10^{17} m^{-2}. During severely disturbed conditions values as high as $8 \cdot 10^{17}$ m^{-2} have been measured at middle latitudes (Taylor, 1966).

With an integrated density of 10^{17} m^{-2} the Faraday rotation for one-way transmission may amount to about 8^{o} for the EISCAT UHF-frequency.

It should be remembered that a density of 10^{17} m^{-2} will only correspond to scattering volumes sufficiently high in the ionosphere that the bulk of ionization is traversed by the radar wave.

In practical terms the Faraday rotation effect is likely to be insignificant for UHF operation at D-,E- and lower F-region heights, except during severe disturbances.

The relation between the rotations experienced at VHF and UHF may be expressed as:

$$\Theta_{VHF} = \Theta_{UHF} \left(\frac{f_{UHF}}{f_{VHF}} \right)^2$$

With $\Theta_{UHF} = 8^{o}$ we obtain:

$$\Theta_{VHF} = 8 \left(\frac{933}{224} \right)^2 = 138^{o}$$

To account for the return passage the values computed above should be doubled.

It is concluded that for the lower EISCAT frequency the Faraday rotation is expected to significantly alter the orientation of the polarization ellipse, even for the lower strata of the ionosphere. By transmitting circular polarization and arranging for reception of the orthogonal mode (monostatic operation only) the optimal scattered power will be recorded.

With the VHF system the Faraday rotation will be exploited for electron density measurements.

By differentiating equation (6.40) we find:

$$N_e = \text{const} \frac{d\Theta(s)}{ds} \qquad (6.41)$$

indicating that the electron density is proportional to the differential of the rotation angle with respect to range.

A practical way of designing a detection scheme for the Faraday rotation effect in incoherent scatter observations has been deviced by Farley(1969). The technique described involves sequencies of circularly polarized pulse transmissions, switching the hand of rotation from pulse to pulse. Upon reception the signals are processed by synchronous detectors. The phase differences, $\phi(s)$, between the two signals are extracted by crosscorrelation. By numerically differentiating the phases stored for adjacent range gates the electron density profiles are derived.

6.7 The EISCAT polarizer

A schematic representation of the EISCAT polarizer is shown in figure 6.10.

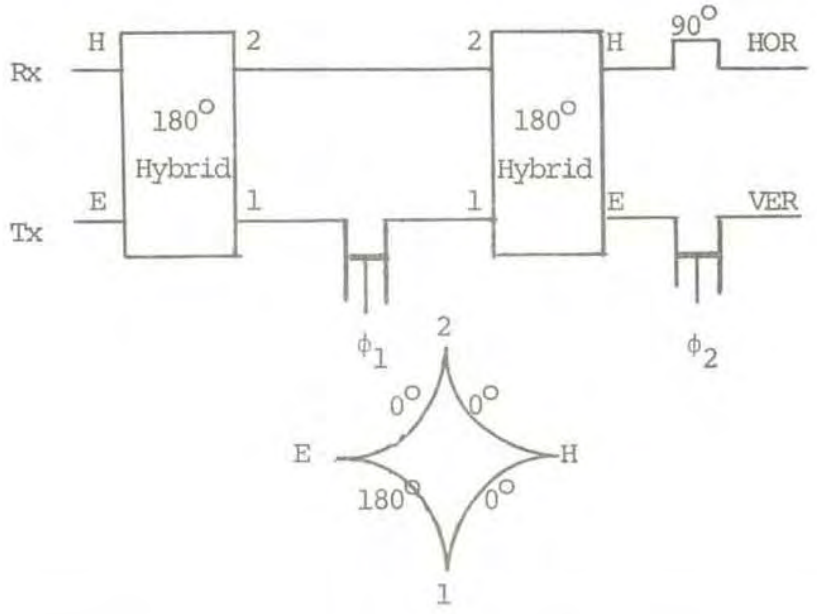

Figure 6.10 The EISCAT polarizer at the transmitter station

The feed design at the remote stations differ from the configuration at Tromsø in that the parametric amplifier at these stations is inserted between the horn (more correctly the OMT - Orhtogonal Mode transducer) and the polarizer. In the Tromsø feed system the polarizer connects directly to the OMT. Through limiter networks one channel of the paramp is coupled to one port of the polarizer, the other channel connects to the duplexer (T/R switch). The polarizer versions also differ in that at Kiruna and Sodankylä they are

realised in coaxial technique, whereas at Tromsø the polariser is designed by use of waveguide components.

The principle of operation of the polarizer is described in volume IV of the "TIW Systems 32 Meter Antenna Operations & Maintenance Manual" and by Hagfors in a recent note entitled "Transmitter Polarizer Control in the EISCAT UHF System".

The polarizer is built with two 180° hybrids and two 180° phase shifters. Phase relations for the hybrids are depicted by the starlike graph of figure 6.10. A signal at the Tx-port of the first hybrid divides in two out-of-phase signals of equal amplitude. The relative phase of the signals feeding the second hybrid is determined by the setting of the first phase shifter. It will also be noted that the amplitudes of the signals appearing at the horizontal and vertical ports of the OMT are defined by the phase shift, φ_1, introduced by the first shifter. The second phase shifter determines the relative phase of the output signals.

We may distinguish between the following polarization modes:

1. Linear polarization

$$\varphi_2 = \begin{cases} 0^{\circ} \\ 180^{\circ} \end{cases}$$

$$\operatorname{tg}\alpha = \frac{E_H}{E_V} = \operatorname{tg}\frac{\varphi_1}{2} \qquad (6.42)$$

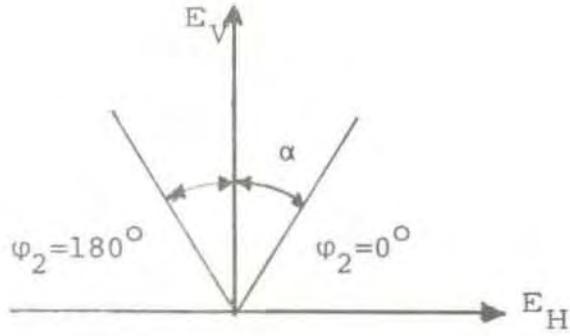

Figure 6.11 Linear polarization

Special cases:

- Horizontal polarization $\varphi_1 = 180^{\circ}$
- Vertical polarization $\varphi_1 = 0^{\circ}$

Note that for $\varphi_1 = 180^{\circ}$ the signal amplitude at the vertical port of the OMT is zero irrespective of the value of φ_2.

2. Circular polarization

- Lefthand $\varphi_1 = \varphi_2 = 90^o$
- Righthand $\varphi_1 = 90^o \quad \varphi_2 = -90^o$

3. Elliptical polarization

From (6.15), (6.16) and (6.18) we readily obtain:

$$\operatorname{tg}\left(\frac{\pi}{2} - \alpha\right) = \operatorname{tg}\beta = 2\cos\varphi_2 \frac{\operatorname{tg}\frac{\varphi_1}{2}}{\left(\operatorname{tg}\frac{\varphi_1}{2}\right)^2 - 1} \qquad (6.43)$$

$$R = \operatorname{cotg}\frac{\varphi_1}{2} \qquad (6.44)$$

$$\left(\frac{B}{A}\right)^2 = \frac{R^2\cos^2\beta + \sin^2\beta - R\sin 2\beta\cos\varphi_2}{R^2\sin^2\beta + \cos^2\beta + R\sin 2\beta\cos\varphi_2} \qquad (6.45)$$

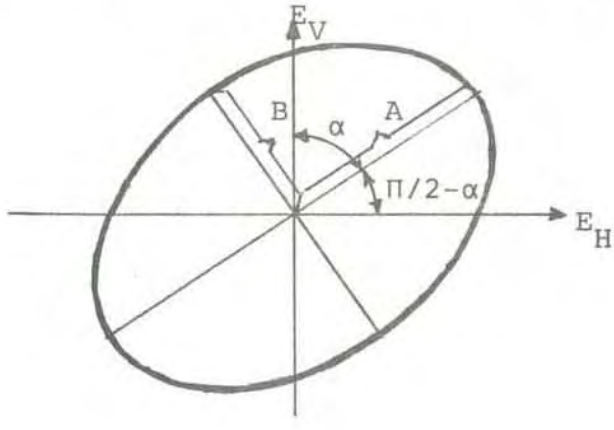

Figure 6.12 Elliptical polarization

For a description of the practical arrangements implemented to control the polarization setting we refer to the Operation & Maintenance Manual.

Matrix representation

In mathematical terms it is convenient to treat the polarizer by use of complex notation and matrix algebra. As shown by Hagfors the output of the hybrid may be written:

$$\vec{f} = \begin{bmatrix} f_2 \\ f_1 \end{bmatrix} = \frac{1}{\sqrt{2}} \begin{bmatrix} 1 & 1 \\ 1 & -1 \end{bmatrix} \begin{bmatrix} e_H \\ e_E \end{bmatrix} = M \begin{bmatrix} e_H \\ e_E \end{bmatrix} \qquad (6.46)$$

the subscripts being in accord with the notation used in the manual.

For the first phase shifter the matrix is given by:

$$N_1 = \begin{bmatrix} 1 & 0 \\ 0 & e^{-j\varphi_1} \end{bmatrix} \qquad (6.47)$$

the effect being to introduce a phase delay in the feed path connecting the ports 1 of the two hybrids.

The matrix of the second phase shifter may be written:

$$N_2 = \begin{bmatrix} -j & 0 \\ 0 & e^{-j\varphi_2} \end{bmatrix} \qquad (6.48)$$

Carrying out the matrix multiplication we obtain the matrix for the entire polarizer unit:

$$P_T = N_2 M N_1 M = \frac{1}{2} \begin{bmatrix} -j(1 + e^{-j\varphi_1}) & -j(1 - e^{-j\varphi_1}) \\ e^{-j\varphi_2}(1 - e^{-j\varphi_1}) & e^{-j\varphi_2}(1 + e^{-j\varphi_1}) \end{bmatrix} \qquad (6.49)$$

Setting $e_H = 0$ and $e_E = 1$ we have:

$$E_H = -j(1 - e^{-j\varphi_1})/2 = -je^{-j\frac{\varphi_1}{2}} \left[\frac{e^{j\frac{\varphi_1}{2}} - e^{-j\frac{\varphi_1}{2}}}{2} \right] = e^{-j\frac{\varphi_1}{2}} \sin\frac{\varphi_1}{2} \qquad (6.50)$$

$$E_V = e^{-j\varphi_2}(1 + e^{-j\varphi_1})/2 = e^{-j\varphi_2} e^{-j\varphi_1/2} \left[\frac{e^{j\varphi_1/2} + e^{-j\varphi_1/2}}{2} \right] =$$

$$e^{-j(\varphi_2 + \varphi_1/2)} \cos(\varphi_1/2) \qquad (6.51)$$

By introducing the time factor $e^{j\omega t}$ and taking the real parts of the expressions we find:

$$E_H = \sin\frac{\varphi_1}{2}\cos(\omega t - \frac{\varphi_1}{2}) \qquad (6.52)$$

$$E_V = \cos\frac{\varphi_1}{2}\cos(\omega t - \frac{\varphi_1}{2} - \varphi_2) \qquad (6.53)$$

which agree with the derivations given in figure 2.4 in the manual.

For reception the polarization matrix is:

$$P = M N_1 M N_2 = \frac{1}{2}\begin{bmatrix} -j(1 + e^{-j\varphi_1}) & e^{-j\varphi_2}(1-e^{-j\varphi_1}) \\ -j(1 - e^{-j\varphi_1}) & e^{-j\varphi_2}(1+e^{-j\varphi_1}) \end{bmatrix} \qquad (6.54)$$

In the following we consider some examples of reception for various settings of the polarizer.

1) Polarizer set for transmission of a linear field at an angle α with the vertical

According to (6.42):

$$\varphi_1 = 2\alpha \qquad (6.55)$$

Let us assume that the incoming field is as given in figure (6.13)

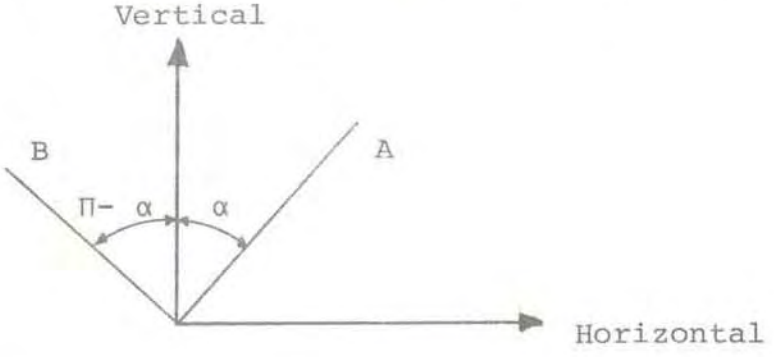

Figure 6.13 Directions of incoming field

Incoming field			
Case	Direction	e_1 (hor)	e_2 (vert)
A	At angle α with vertical	$\frac{-je^{j\varphi_1/2}}{2}(1-e^{-j\varphi_1})$	$\frac{e^{j\varphi_1/2}}{2}(1+e^{-j\varphi_1})$
B	At angle $\pi/2-\alpha$ with vertical	$\frac{-e^{j\varphi_1/2}}{2}(1+e^{-j\varphi_1})$	$\frac{-je^{j\varphi_1/2}}{2}(1-e^{-j\varphi_1})$

Output		
Case	Tx-port	Rx-port
A	$e^{-j\varphi_1/2}$	0
B	0	$e^{-j\varphi_1/2}$

Note that the angle α is determined by the tristatic scatter geometry and the field direction which optimizes the reception at the two remote station (possibly with the Faraday rotation taken into account).

2) Reception of circular polarization. Polarizer set up for transmission of a righthand wave.

$\varphi_1 = 90^\circ$ $\varphi_2 = -90^\circ$

Incoming wave			Output	
Sense of rotation	e_1 (hor)	e_2 (vert)	Tx-port	Rx-port
Lefthand	1	j	0	-(1+j)
Righthand	1	-j	(1-j)	0

We notice that to have the signal power appearing at the Tx-port requires that the antenna is configured for transmission of the same polarization as pertaining to the incoming wave.

3) Reception of elliptical polarization, provided a circular wave is transmitted

We assume that the receiver antenna is set up for transmission of an elliptical wave-field as given by (6.50) and (6.51).

We may write for the complex vector describing the ellipse:

$$\vec{E} = -\frac{j}{2}\,(1 + e^{-j\varphi_1})\,\hat{i}_H + \frac{e^{-j\varphi_2}}{2}\,(1 - e^{-j\varphi_1})\,\hat{i}_V \qquad (6.56)$$

$\hat{i}_H$ and $\hat{i}_V$ being unit vectors in the horizontal and vertical directions.

If the incoming wave describes an ellipse identical to that defined by (6.56) signal power will appear at both the Rx- and the Tx-ports. To ascertain that all the signal power shall appear at one port only, the incoming field ellipse must be orthogonal to the antenna polarization ellipse.

To obtain the orthogonal vector of the vector (6.56) we take the vector product.

$$\vec{E}_{orth} = \overline{E} \times \overline{n} \qquad (6.57)$$

where $\overline{n}$ is a unity vector defined as

$$\overline{n} = \hat{i}_H \times \hat{i}_V \qquad (6.58)$$

$$\vec{E}_{orth} = \frac{1}{2}\left[e^{-j\varphi_2}(1 - e^{-j\varphi_1})\hat{i}_H + j(1 + e^{-j\varphi_1})\,\hat{i}_V \right] \qquad (6.59)$$

By multiplication with the receiver matrix:

$$\vec{E}_R = \begin{bmatrix} -je^{-j\varphi_1} \\ 0 \end{bmatrix} \qquad (6.60)$$

Reverting to real expressions:

$$E_{Rx} = \sin(\omega t - \varphi_1) \qquad (6.61)$$

$$E_{Tx} = 0 \qquad (6.62)$$

In practical terms the procedure of matching the antenna to the incoming elliptical wave will be:

(i) From the geometry of the problem determine the axial ratio and the direction of the major axis of the ellipse (see 6.5.2), assuming a circular transmitted field (and neglecting Faraday rotation).

(ii) Specify the orthogonal ellipse by rotating the received field ellipse through 90°.

(iii) Use relations (6.43) to (6.45) to determine the setting of the phase changers of the polarizer.

We note that the power of the elliptical signal field will be recorded by setting the polarizer for right- or lefthand circular polarization and measuring the signals at both the Rx and the Tx-port. Figure 6.8 displays the loss incurred by recording only the dominating element of the two circular components of which the ellipse is composed.

6.8 Discussion and conclusions

In analysing the polarization problem in tristatic operation there are three general, partly irreconcilable, requirements:

(i) The polarization should be selected so as to optimize the received scatter power

(ii) The polarization setting should be simple, involving as little as possible of on-line computational efforts and mechanical operations within the polarizer

(iii) For the subsequent data analyses the reception should preferably be "matched", in the sense that the essential part of the signal power should appear at one port of the polarizer

The following comments are partly made by general considerations and

partly by assessment of the results displayed by figure 6.5, 6.7 and 6.8.

1) For the transmitter station the requirement under (i) is met irrespective of which polarization is selected. For linear and circular polarization the matching requirement (iii) is also satisfied for this station in the case of no Faraday rotation. With Faraday rotation matching can only be achieved in general with circular polarization. With linear polarization matching would necessitate reconditioning the polarizer during the time interval between transmission of a pulse and the reception. Moreover, a continuous reconditioning of the polarizer would be required if several height ranges should be explored. Technically this is not feasible.

2) For the lower height regions linear polarization is the one that best satisfies (i) for the two remote stations.

3) Linear polarization does not meet the conditions labelled (ii) above. To optimize the received power would require resetting the polarizers at all three sites each time the coordinates for the scatter volume were changed, preferably by reading precalculated arrays of location/field-direction relationships. A possible simplification may be obtained by relaxing the requirement for continuous optimization and keeping the polarizer setting constant within reasonably large cells in the three-dimensional array structure. If Faraday rotation is to be included several arrays would have to be filed, prescribing the required adjustment as a function of electron density.

4) Since a transmitted circular wave in general appear at the remote stations as elliptically polarized, the matching requirement (iii) at these stations would involve resetting of the polarizers each time the position of the scatter volume changed, allowing for the associated alterations in the orientation and form of the received ellipse. By adopting the simpler procedure of processing only the dominating circular mode one avoids resetting the polarizer (except possibly for the rare events when 2χ goes through 90°) at any site. This is the mode of operation which best meets with condition (ii).

5) According to figure 6.8, for heights above 300 km no appreciable amount of power is lost by recording only the dominating circular mode at the remote stations.

6) For heights above 3-400 km little is gained by retaining linear polarization for the Kiruna station. Even for a height of 100 km the benefit of the linear polarization tends to become insignificant for latitudes above 70-71° N. Since the distance Tromsø/Sodankylä is about twice the distance Tromsø/Kiruna for Sodankylä linear polarization retains it advantage over circular polarization to larger heights and over larger spans of latitude and longitude. However, above 600 km the benefit of linear polarization tends to diminish even for this station.

7) It should be emphasized that Faraday rotation is essentially a problem with linear polarization (it will introduce difficulties with matched elliptical reception in the circular transmission mode) with the scatter volume remotely located (at high altitudes or at long distances in oblique geometry). As demonstrated by the computed figures, and underlined in the preceding paragraphs, the benefit of linear polarization decreases with increasing distance to the scatter volume. We are therefore in a somewhat favourable position, that these two effects tend to counteract.

In the discussion in this section we have dealt only with linear and circular transmitted waves. We might conceive of selected events when someone would like to transmit elliptically polarized waves, f.inst. with the purpose of removing the ellipticity of the remotely received waves. It appears to the author, though, that these are likely to be rare and exclusive incidents without much practical significance.

References

Farley D T - Radio Science 4
143 (1969)

Hagfors T - Transmitter Polarizer Control in the EISCAT UHF System, EISCAT Note (1979)

Kales M L - Proceedings IRE
544 (1951)

Kraus J D - Radio Astronomy,
McGraw-Hill Book Company (1966)

Murdin J - SNR for the EISCAT UHF System,
KGI Report No 78:1 (1978)

Sichak W and Milazzo S - Proceedings IRE
997 (1948)

Taylor G N - Electron Density Profiles in the Ionosphere & Exophere, Ed. J Frihagen,
North-Holland Publ. Company (1966)

7 VHF ANTENNA SWITCHYARD

As indicated in the sketch below the VHF antenna consists of four 40 x 30 m panels, each panel furnished with its own motor drive, facilitating independent movements of the sections in the magnetic meridian plane.

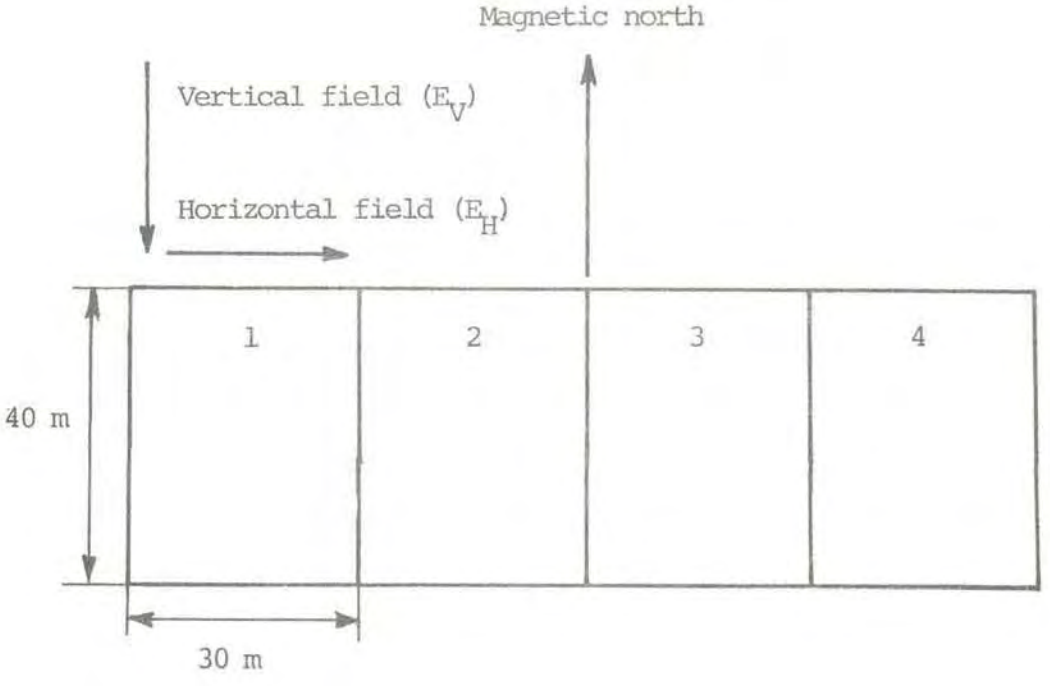

Figure 7.1 VHF antenna configuration

The mechanical flexibility cannot be fully exploited with the transmit/receive system as presently configured. It will, however, in addition to single beam operation, accomodate a dual-beam mode, with panels 1 & 2 and 3 & 4 acting as independent antennas. The selection of the single-beam or dual-beam option is accomplished by an automatic switchyard.

The switchyard is located on a concrete pad at the centre of the antenna base. The construction, delivered by Spinner (Germany), is realized in coaxial technique (approximate diameter of the coaxial line 300 mm), and includes two 90° hybrids, two motor-driven switches and feed paths as indicated in figure 7.2 below.

An array of crossed dipoles, with axes parallel and transverse to the antenna axis provide the horizontal and vertical field components as indicated in figure 7.1.

7.1 Schematic layout and working principle

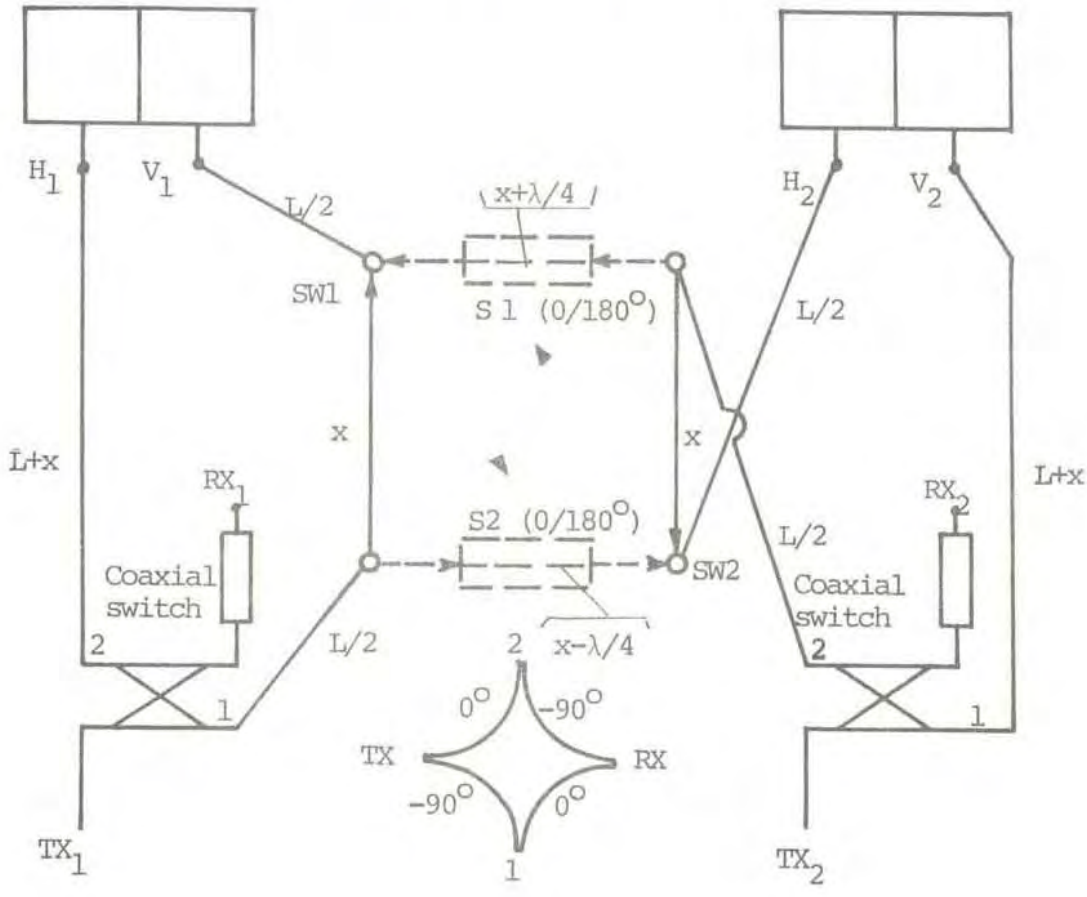

Figure 7.2 Schematic presentation of VHF antenna switchyard

With the switching elements SW 1 and SW 2 in the indicated positions the antenna is configured for dual-beam operation, transmitter 1 and 2 feeding antenna sections 1 & 2 and 3 & 4 respectively. Note that the phase paths for the vertical and horizontal dipole arrays have the same lengths. This means that the phase quadrature pertaining to the horizontal and vertical field components at the hybrid outputs is retained also at the dipole terminals.

With the switches SW 1 and SW 2 in the alternative positions (indicated by dashed lines) the antenna is set up for single-beam radiation. In this case the entire horizontal and vertical dipole arrays are fed by transmitter 1 and 2 respectively. Note that in this case the phase paths for the two horizontal and the two vertical feeds differ by $\lambda/4$ (or 90°). The elements S 1 and S 2, indicated in the drawing, introduce phase delays of 0° or 180°. These elements are not installed in the switchyard as presently configured, but are considered as worthwhile modifications at a later stage (see note by Hagfors, labelled SAC 15.12).

7.1.1 Transmission in single-beam operation

An equivalent scheme for the single-beam operation is depicted in figure 7.3.

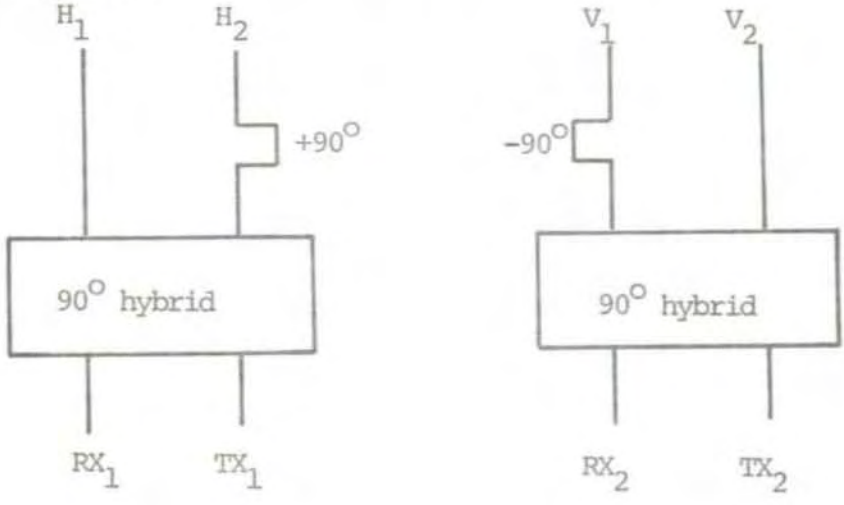

Figure 7.3 Equivalent representation

Let us denote the transmitting matrices corresponding to hybrids and subsequent phasing elements M_1 and M_2.

We have:

$$\vec{f}_1 = M_1 \vec{e}_1 \tag{7.1}$$

$$\vec{f}_2 = M_2 \vec{e}_2 \tag{7.2}$$

where

$$\vec{f}_1 = \begin{bmatrix} e_{H_1} \\ e_{H_2} \end{bmatrix}, \quad \vec{f}_2 = \begin{bmatrix} e_{V_1} \\ e_{V_2} \end{bmatrix} \tag{7.3}$$

$$\vec{e}_1 = \begin{bmatrix} e_{RX_1} \\ e_{TX_1} \end{bmatrix}, \quad \vec{e}_2 = \begin{bmatrix} e_{RX_2} \\ e_{TX_2} \end{bmatrix} \tag{7.4}$$

and

$$M_1 = \frac{1}{\sqrt{2}} \begin{bmatrix} -j & 1 \\ j & 1 \end{bmatrix}, \quad M_2 = \frac{1}{\sqrt{2}} \begin{bmatrix} -1 & -j \\ 1 & -j \end{bmatrix} \tag{7.5}$$

Consider the following cases:

(i) $$e_{TX_1} = e_{TX_2} = 1 \tag{7.6}$$

$$e_{RX_1} = e_{RX_2} = 0 \tag{7.7}$$

Henceforth we assume that condition (7.7) is always fulfilled.

We obtain:

$$\begin{bmatrix} e_{H_1} \\ e_{H_2} \end{bmatrix} = \frac{1}{\sqrt{2}} \begin{bmatrix} 1 \\ 1 \end{bmatrix} \tag{7.8}$$

$$\begin{bmatrix} e_{V_1} \\ e_{V_2} \end{bmatrix} = \frac{1}{\sqrt{2}} \begin{bmatrix} -j \\ -j \end{bmatrix} \tag{7.9}$$

$$\frac{e_{V_1}}{e_{H_1}} = \frac{e_{V_2}}{e_{H_2}} = -j \tag{7.10}$$

The antenna radiates lefthand <u>circular</u> polarization.

(ii) $$e_{TX_1} = 1 \qquad e_{TX_2} = -1 \tag{7.11}$$

In this case the polarization is <u>righthand</u> circular.

In conducting Faraday rotation experiments with the VHF radar it might be desirable to alter the hand of the circular polarization from pulse to pulse. From the derivations above it will be seen that this requires altering the phase of one of the transmitted signals by 180° from pulse to pulse (we assume that the phase is changed in <u>one</u>

feed line only).

(iii) $e_{TX_1} = 1 \qquad e_{TX_2} = \pm j$ (7.12)

Performing the matrix multiplications we find:

$$\frac{e_{V_1}}{e_{H_1}} = \frac{e_{V_2}}{e_{H_2}} = \pm 1 \tag{7.13}$$

corresponding to linear polarization with the plane of polarization inclined $\pm 45^{o}$ with respect to the vertical axis.

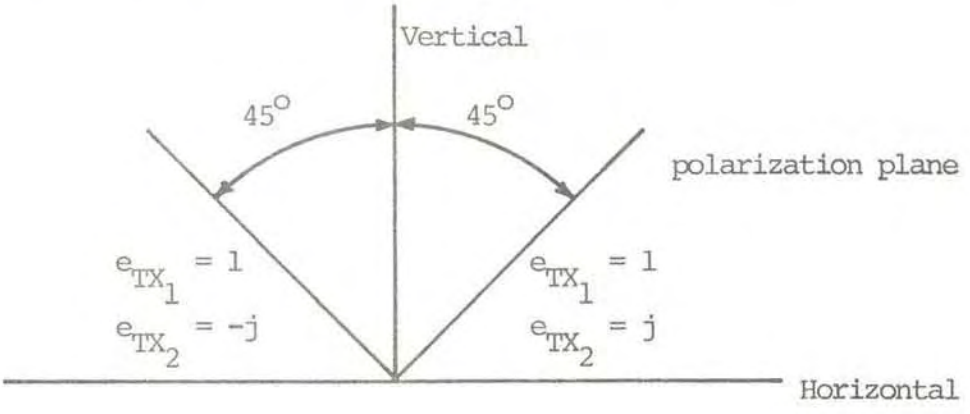

Figure 7.4 Linear polarizations in single-beam operation

7.1.2 Transmission in dual-beam mode

Schematic representation of the polarizing networks for dual-beam transmission is shown in figure 7.5.

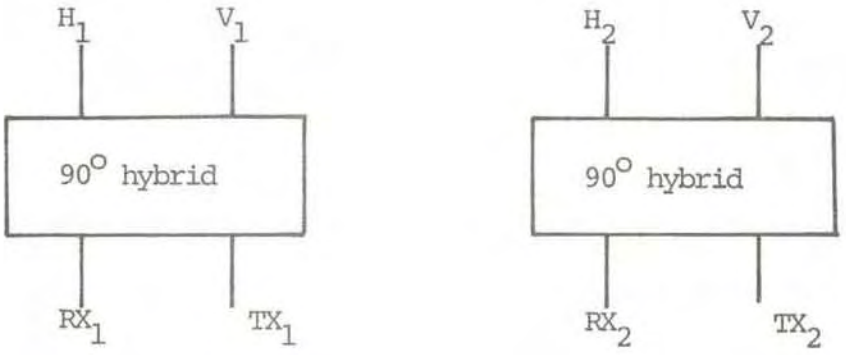

Figure 7.5 Switchyard representation in dual-beam operation

With

$$\vec{f}_1 = \begin{bmatrix} e_{H_1} \\ e_{V_1} \end{bmatrix} \qquad \vec{f}_2 = \begin{bmatrix} e_{H_2} \\ e_{V_2} \end{bmatrix} \tag{7.14}$$

and

$$\vec{e}_1 = \begin{bmatrix} e_{RX_1} \\ e_{TX_1} \end{bmatrix} \qquad \vec{e}_2 = \begin{bmatrix} e_{RX_2} \\ e_{TX_2} \end{bmatrix} \tag{7.15}$$

the transmission matrices become:

$$M_1 = M_2 = \frac{1}{\sqrt{2}} \begin{bmatrix} -j & 1 \\ 1 & -j \end{bmatrix} \tag{7.16}$$

In this case we <u>always</u> have:

$$\frac{e_{V_1}}{e_{H_1}} = \frac{e_{V_2}}{e_{H_2}} = -j \tag{7.17}$$

For both antenna halves the transmissions are <u>lefthand</u> circular irrespective of the phases of the signals at the hybrid input ports.

Polarization flipping, or transmissions with linear polarizations, are not possible in dual-beam operation.

7.2 Reception

7.2.1 Single-beam

Matrices (figure 7.3):

$$R_1 = \frac{1}{\sqrt{2}} \begin{bmatrix} -j & j \\ 1 & 1 \end{bmatrix} \tag{7.18}$$

$$R_2 = \frac{1}{\sqrt{2}} \begin{bmatrix} -1 & 1 \\ -j & -j \end{bmatrix} \tag{7.19}$$

In this case we find that all the signal power appears at the TX_1- and TX_2-ports irrespective of whether the polarization is circular or linear.

Let us now assume that the switchyard had been equipped with the extra phasing elements S 1 and S 2 (figure 7.2), programmed to present 0^o phase change to an outgoing signal but 180^o to an incoming wave.

Now the reception matrices are:

$$R_1 = \frac{1}{\sqrt{2}} \begin{bmatrix} -j & -j \\ 1 & -1 \end{bmatrix} \tag{7.20}$$

$$R_2 = \frac{1}{\sqrt{2}} \begin{bmatrix} 1 & 1 \\ j & -j \end{bmatrix} \tag{7.21}$$

As examples we select:

(i) $$e_{V_1} = e_{V_2} = \pm j \tag{7.22}$$

$$e_{H_1} = e_{H_2} = 1 \tag{7.23}$$

representing a lefthanded (+) or righthanded (-) circularly polarized wave.

We find:

$$\begin{bmatrix} e_{RX_1} \\ e_{TX_1} \end{bmatrix} = \frac{1}{\sqrt{2}} \begin{bmatrix} -j & -j \\ 1 & -1 \end{bmatrix} \begin{bmatrix} 1 \\ 1 \end{bmatrix} = -\sqrt{2} \begin{bmatrix} j \\ 0 \end{bmatrix} \tag{7.24}$$

and

$$\begin{bmatrix} e_{RX_2} \\ e_{TX_2} \end{bmatrix} = \frac{1}{\sqrt{2}} \begin{bmatrix} 1 & 1 \\ j & -j \end{bmatrix} \begin{bmatrix} \pm j \\ \pm j \end{bmatrix} = +\sqrt{2} \begin{bmatrix} \pm j \\ 0 \end{bmatrix} \tag{7.25}$$

(ii) $e_{V_1} = e_{V_2} = e_{H_1} = e_{H_2} = 1$ (7.26)

corresponding to a linear field propagating in the antenna broadside direction.

We obtain:

$$\begin{bmatrix} e_{RX_1} \\ e_{TX_1} \end{bmatrix} = -\sqrt{2} \begin{bmatrix} j \\ 0 \end{bmatrix} \tag{7.27}$$

$$\begin{bmatrix} e_{RX_2} \\ e_{TX_2} \end{bmatrix} = -\sqrt{2} \begin{bmatrix} 1 \\ 0 \end{bmatrix} \tag{7.28}$$

We see that in both cases (i) and (ii) the entire signal power appears at the receiver ports of the switchyard.

7.2.2 Dual-beam

The receiver matrix is given by (7.16).

According to the findings in 7.1.2 the transmitted waves are always lefthand circular, leading to righthand polarization of the incoming scattered field.

We obtain:

$$\begin{bmatrix} e_{RX_1} \\ e_{TX_1} \end{bmatrix} = \begin{bmatrix} e_{RX_2} \\ e_{TX_2} \end{bmatrix} = -\sqrt{2} \begin{bmatrix} j \\ 0 \end{bmatrix} \qquad (7.29)$$

Again we find that the power is avaiable at the receiver port.

7.3 Feed system beyond the switchyard

In figure 7.6 is shown a sketch of the power distribution network beyond the switchyard. (From "Request for Proposal" (VHF-antenna)).

We note that:

(i) The primary radiating system consists of 128 crossed dipoles, 32 dipoles for each of the four panels. Figure 7.6 shows the coaxial line system for one polarization (horizontal or vertical) for one panel. Level C in the lower lefthand portion of the scheme corresponds to the feed points labelled V_1 or H_1 (V_2 or H_2) in the switchyard presentations depicted in the preceding part of this chapter.

(ii) The ultimate distribution element is a 3 dB directional coupler with a dummy load. When the beam is in the broadside direction the phase paths for all dipoles are equal. In this case no power is dissipated in the dummy load. By systematically increasing the phase paths (by manually replacing cables) along the dipole array, it will be possible to steer the beam up to 24° from the broadside direction. This type of beam steering will be associated with an increase in the VSWR at the dipole terminals (Egil Hauger, "Phased Linear Array", EISCAT VHF-antenna document). A part of the reflected power will be dissipated by the dummy load (for scan angles of 20° all the reflected power will be dissipated by the dummy load) (Kildal "Feeder Elements for the EISCAT VHF Parabolic Cylinder Antenna"). The rest of the reflected power will be coupled to the output and input ports of subsequent power dividers. A part of the reflected power may also appear at the RX-ports of the switchyard. It is difficult to assess

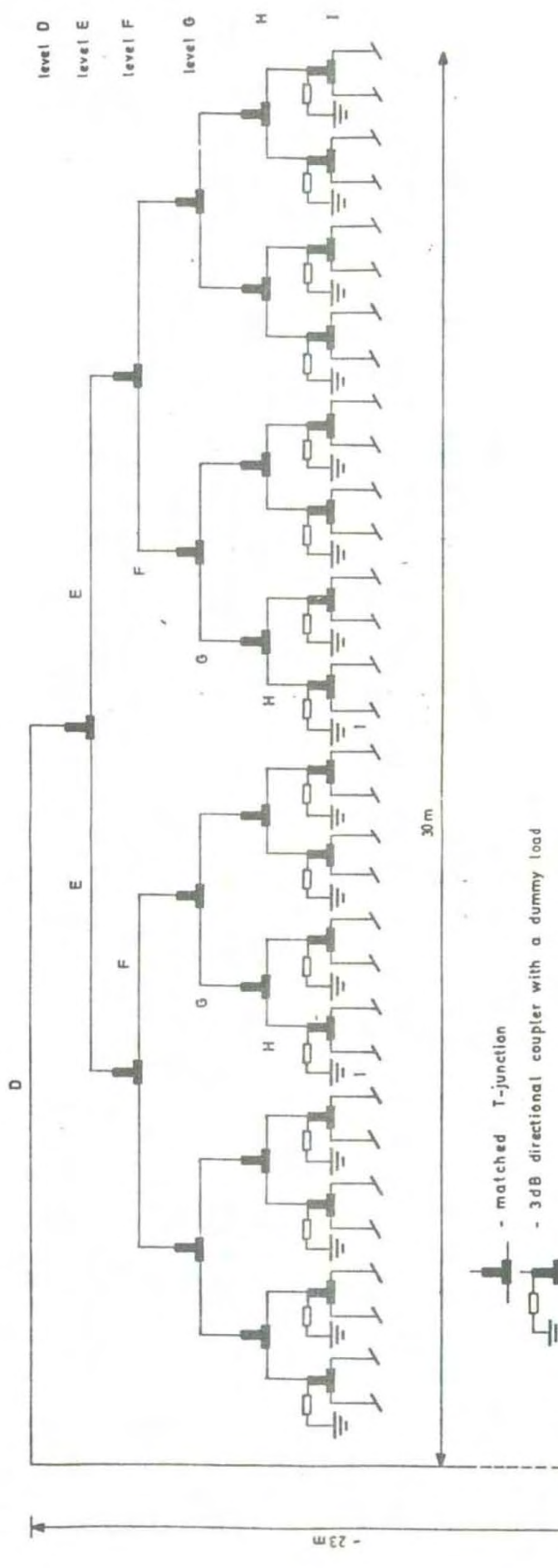

Figure 7.6 Power distribution network beyond switchyard

the amount of power which may couple to the RX-port under these circumstances. It has been suggested that the specification of the power which the coaxial T/R-switches must handle, should be postponed until measurements have been made on the complete antenna (Hagfors SAC 15.12). An option which is considered, is to move two pin-diode switches delivered as integral parts of the VHF-antenna duplexer to the switchyard and let them serve as the receiver protectors.

7.4 Discussion

It emerges from the derivations in sections 7.2.1 and 7.2.2 that with the present system (without the 180° phasing elements) the scattered signal power in Single-Beam operation appears at the TX-ports of the switchyard, whereas the power will be available at the RX-ports in the Dual-Beam mode. This means that the receivers must be relocated each time one goes from one operational mode to the other. In the Single-Beam mode the receivers must connect to the receiver ports of the duplexer in the transmitter hall, whereas in Dual-Beam operation they would have to be at the switchyard location.

The major advantage of having the 180° phasing elements inserted in the system is that one thereby dispenses with the necessity of relocating the receivers by making the power appear at the RX-ports also in the Single-Beam mode.

A drawback with the installation of the extra phasing elements may be the differential damping thereby introduced in the two feed lines branching off each hybrids (extra damping in H_2 and V_2 lines).

In transmission this will tend to somewhat distort the polarization behaviour in that the horizontal and vertical amplitudes at the two antenna halves are not exactly equal. In reception the differential damping will cause a fraction of the received power to appear at the TX-ports. With a receiving system designed to monitor the effect at <u>one</u> port only (at each hybrid), the power at the TX-ports will be lost.

Until we know the characteristics of the phasing elements possibly

to be installed, we cannot assess how serious the effect of the differential damping will be. It is likely, though, that the damping will increase with increasing deviation from the transmitted frequencies, therefore being more of a problem for plasma-line reception (at 5-10 MHz from the transmission frequencies) than for ion-line detection.

References:

Hagfors, T - EISCAT document, SAC 15.12 (July 1979)

Hauger, E - In "Phased Linear Array - Fixed Reflector Concept for the EISCAT VHF Antenna" (1977)

Kildal, P-S - Feeder Elements for the EISCAT VHF Parabolic Cylinder Antenna, EISCAT Technical Notes 78/8 (1978)

- Request for Proposal (VHF Antenna, 1977)

PARAMETRIC AMPLIFIERS

8.1 Introduction

Parametric amplifiers find their use in low noise applications. The key element in many practical amplifiers is a specially designed p-n junction, termed varactor diode or simply varactor. This may be operated at temperatures below room temperature, opening a possibility for diminishing the termal noise by cooling techniques.

In the following we first briefly introduce the amplifying process by studying a simple L-C circuit. We thereafter go on to consider a more general scheme for power amplification.

8.2 Simple mechanism for energy transfer

Consider the resonance tank of figure 8.1

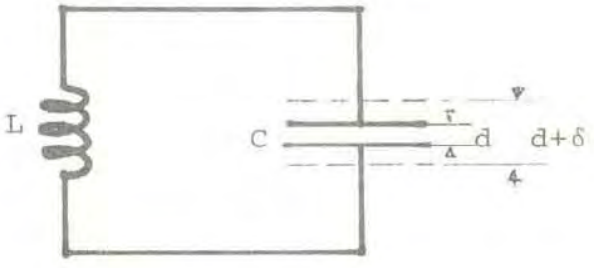

Figure 8.1 L-C circuit with variable frequency

Suppose that the plates of the condenser are pulled apart, by an additional distance δ, each time the condenser voltage goes through a positive or negative maximum.

Work must be done in separating the charges on the plates. The energy is transferred to the electric field between the plates. By increasing the distance between the capasitor plates the capacitance is reduced. According to the formula $V = q/C$, where V is voltage, q the capacitor charge and C the capacitance, we find that the capacitor voltage is enhanced by the repositioning of the plates.

Let us further assume that the plates are pushed back to their original position each time the charge on the plates is zero. No energy is required for this operation. Figure 8.2 illustrates the mechanism described. The net result is an increase of the energy (and the oscillator voltage) of the tank circuit, the energy provided by the pump, periodically changing the plate distance at twice the oscillator frequency.

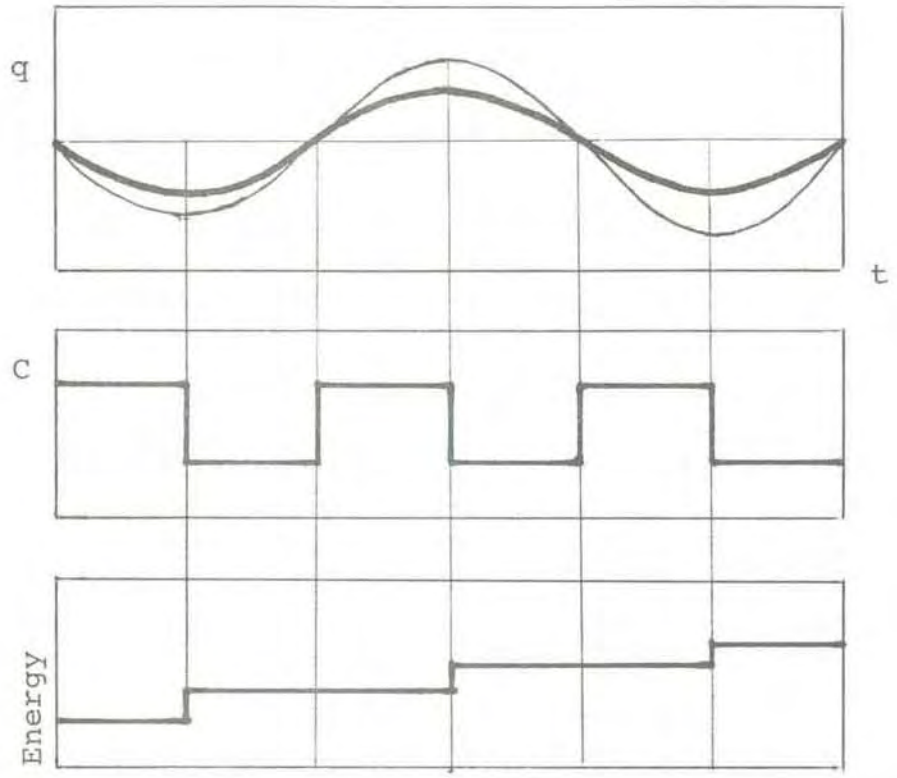

Figure 8.2 Effect of varying the spacing between the parallel capacitance plates

In the simple example we have studied here we note that there must be a fixed relationship between pump and oscillator signals to effect the energy buildup. This restriction may be removed by adding a second tank and letting the variable capacitance be the coupling element between the two tank circuits. The second circuit is often termed the idler, the idling frequency being the difference between the pump and signal frequencies. We will not elaborate on this circuit extension here, but instead focus our attention on some general relations for power transfer.

8.3 Power amplification

We let the sinusoidal input voltage and current of the amplifier shown in figure 8.3 be represented in the conventional way as the real parts of the complex voltage and current:

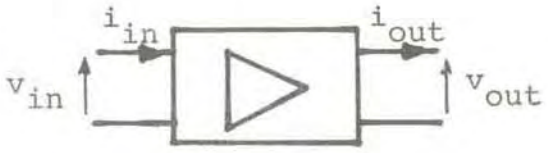

Figure 8.3 Schematic of power amplifier

$$v_{in}(t) = R_e\{ V_{in} \exp(j\omega t) \} \qquad (8.1)$$

$$i_{in}(t) = R_e\{ I_{in}\exp(j\omega t) \} \tag{8.2}$$

where V_{in} and I_{in} are complex amplitudes. The input power is:

$$P_{in} = \tfrac{1}{2}\, Re\{ V_{in}I_{in}^{*} \} \tag{8.3}$$

I_{in}^{*} is the conjugate of the complex current amplitude.
We assume that the output voltage v_{out} and current i_{out} can be represented by a constant term and a series of sinusoidal terms as follows:

$$v_{out}(t) = V_o + Re\{\sum_{m=o}^{\infty}\sum_{n=-\infty}^{\infty} V_{m,n}\exp(j\omega_{m,n}t) \} \tag{8.4}$$

$$i_{out}(t) = I_o + Re\{\sum_{m=o}^{\infty}\sum_{n=-\infty}^{\infty} I_{m,n}\exp(j\omega_{m,n}t) \} \tag{8.5}$$

where $\omega_{m,n} = m\omega_2+n\omega_1$. The frequency ω_2 is independent of the signal frequency ω_1. m and n are integers , m being summed over positive values only. Average output power:

$$P_{out} = \overline{v_{out}(t)\, i_{out}(t)} = P_o + \sum_{m=0}^{\infty}\sum_{n=-\infty}^{\infty} P_{m,n} \tag{8.6}$$

$$P_{m,n} = \tfrac{1}{2}\, Re\, (V_{m,n}I_{m,n}^{*}) \tag{8.7}$$

If any of the power terms $P_{m,n}$ which depends upon the input frequency ($n \neq 0$) is greater than P_{in}, the circuit can be considered to be a power amplifier. In a conventional AC amplifier power gain is achieved by conversion from DC power. However, power amplification can also be obtained by conversion from power at the independent frequency ω_2.

We may distinguish between the following cases:

(i)	$n = 1, m = 0$	parametric amplification
(ii)	$\|n\| = 1, m \geq 1$	frequency changing, mixing
(iii)	$n > 1, m = 0$	harmonic frequency generation, frequency multiplication

In case (ii) the circuit is also termed a parametric converter.

8.4 The parametric element

Nonlinear resistances as well as reactances may serve as parametric circuit elements. We will consider the important case where the parametric component consists of a nonlinear capacitance. Figure 8.4 exhibits a nonlinear q-v characteristic where q is capacitor charge and v the voltage.

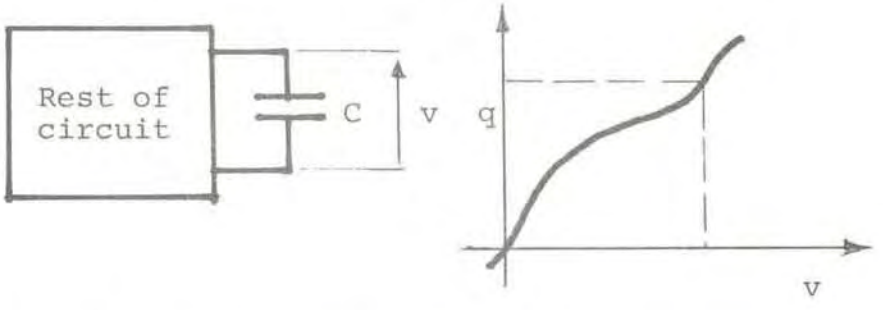

Figure 8.4 Nonlinear charge-voltage characteristic

The charge and voltage may be considered to consist of two terms:

$$q = q_p + q_q \tag{8.8}$$

$$v = v_p + v_q \tag{8.9}$$

v_p and q_p represent voltage and charge when only the pump signal is applied. v_q and q_q include all frequency components due to the application of the input signal to the pumped circuit. We assume that the pump signal is much greater than the input signal. For sufficiently small input signal we have:

$$q = q_p + \left(\frac{dq}{dv}\right)_{q=q_p} v_q \tag{8.10}$$

$$q_q = \left(\frac{dq}{dv}\right)_{q=q_p} v_q \tag{8.11}$$

$$i_q = \frac{d}{dt}\left\{\left(\frac{dq}{dv}\right)_{q=q_p} v_q\right\} \tag{8.12}$$

The incremental capacitance is defined as:

$$C(t) = \left(\frac{dq}{dv}\right)_{q=q_p} \tag{8.13}$$

With the approximations made, C(t) does not depend upon the signal applied. The relations quoted above are therefore linear time varying forms.

Energy is defined as the area under the q-v curve:

$$E = \int_0^q v\,dq \tag{8.14}$$

8.5 Manley-Rowe equations

The power flow in and out of the nonlinear devices at different frequencies are governed by certain constraints. In the case of nonlinear resistances they are described by Page's equations. A corresponding set of relations exists for nonlinear energy storing, lossless devices (reactances), termed the Manley-Rowe equations. They are quoted below without proof:

$$\sum_{k=0}^{\infty}\sum_{m=-\infty}^{\infty} \frac{kP_{k,m}}{\omega_{k,m}} = 0 \tag{8.15}$$

$$\sum_{k=0}^{\infty}\sum_{m=-\infty}^{\infty} \frac{mP_{k,m}}{\omega_{k,m}} = 0 \tag{8.16}$$

where $P_{k,m}$ is the power flowing into the nonlinear capacitance at a frequency $\omega_{k,m} = k\omega_q + m\omega_p$.

A schematic illustrating the use of the Manley-Rowe equations is given in the figure below.

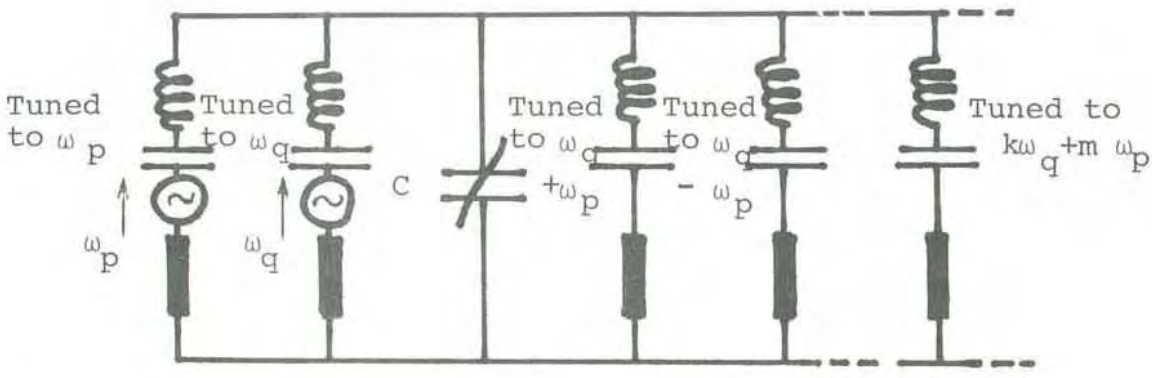

Figure 8.5 Circuit illustrating the use of the Manley-Rowe equations

As an example we consider a circuit where power is allowed to flow only at the signal frequency ω_q, the frequency ω_p and at the general idler frequency $r\omega_p + \omega_q$. The Manley-Rowe equations in this case reduce to:

$$\frac{P_{1,o}}{\omega_q} + \frac{P_{1,r}}{\omega_q + r\omega_p} = 0 \qquad (8.17)$$

$$\frac{P_{1,o}}{\omega_p} + \frac{rP_{1,r}}{\omega_q + r\omega_p} = 0 \qquad (8.18)$$

By convention power flowing into the nonlinear capacitor is positive. From the first equation we find:

$$\frac{P_{1,r}}{P_{1,o}} = -\frac{\omega_q + r\omega_p}{\omega_q} \qquad (8.19)$$

Power $P_{1,o}$ absorbed by the capacitor results in power flowing out of the capacitor at the frequency $\omega_q + r\omega_p$. If $r>1$ the circuit acts as an upper-sideband converter, with the maximum gain being equal to the ratio between the upper-sideband frequency and the signal frequency, irrespective of circuit configuration and degree of nonlinearity.

If $r<0$ and $\omega_q + r\omega_p<0$ both $P_{1,0}$ and $P_{1,r}$ turn out to be negative and the amplifier may show negative resistance at the signal and idler ports. In this case, with a negative resistance amplifier, the capacitor supplies power at both the signal and the idler frequencies.

8.6 Capacitance of a reversed-biased p-n junction

In a parallel-plate capacitor electric charge is stored on conductors bounding an insulating layer. There are no charges in the insulator affecting the electric field and the differential capacitance remains constant

$$C = dq/dv = q/v \tag{8.20}$$

Now let us consider a monocrystal p-n semiconductor junction. As a result of majority carrier diffusion (holes in p-type and electrons in n-type materials) there will be a region in the vicinity of the junction partly depleted of free carriers. However, the uncompensated impurity atoms, positive in the n-type and negative in the p-type regions, result in a space charge double layer and an electric field directed from the n-type to the p-type side of the junction. The field varies with distance from the junction, being greatest at the changover plane.

The amount of uncompensated space charge depends upon the bias voltage, a reverse-bias voltage increasing the depletion-layer width, a forward-bias having the inverted effect. It follows that the depletion-layer capacitance

$$C(v) = dq/dv \tag{8.21}$$

varies with variations in the bias voltage.

To obtain an expression for the depletion layer capacitance the variation of the impurity atom density distribution in the junction region must be known. Models for the p-n junction apply both abrupt and linearly graded density distributions. A typical C_d-V characteristic is depicted in figure 8.6. (The subscript d in C_d denotes "depletion").

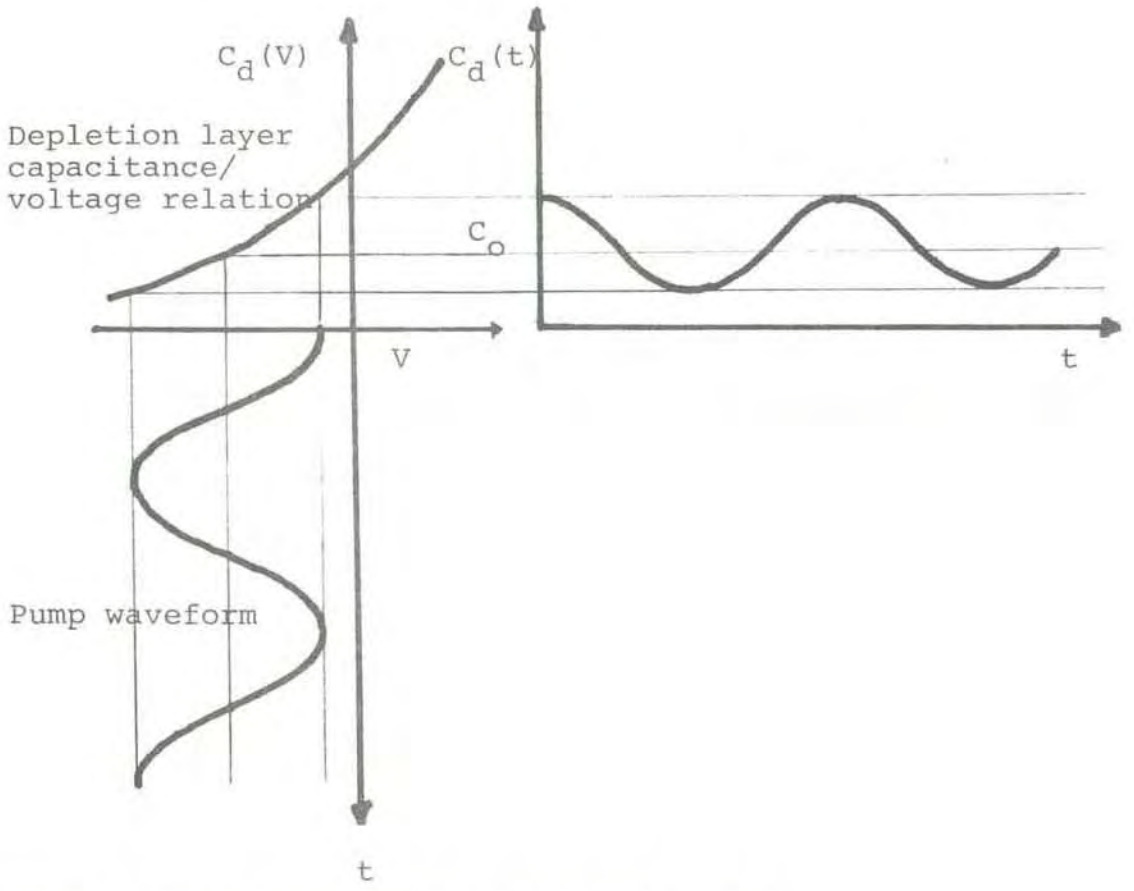

Figure 8.6 Voltage pumping of p-n junction varactor

The periodically varying time dependent capacitance, $C_d(t)$, may be resolved into a Fourier series:

$$C_d(t) = C_o\left(1 + \sum_{n=1}^{\infty} C_n \cos(n\omega_p t)\right) \tag{8.22}$$

$$C_n = 2\,\gamma_n = \frac{1}{\pi C_o}\int_{-\pi}^{\pi} C_d(t)\cos(n\omega_p t)\,d(\omega_p t) \tag{8.23}$$

The time varying component is included in the right-hand summation term. The value of the coefficient γ_n, in particular γ_1, determine the performance of the parametric amplifier. The largest value of γ_1 is always sought. γ_1 is a most essential quantity in elaborations to establish figures of merit of parametric amplifiers. Another key term is R_d, the series resistance of the p-n junction. The angular cut-off frequency is that frequency at which the capacitive reactance equals the series resistance:

$$\omega_c = \frac{1}{C_o R_d} \tag{8.24}$$

8.7 Design considerations

In figure 8.7 is shown a scheme for operating a one-port negative-resistance amplifier, the most common of all parametric amplifier devices.

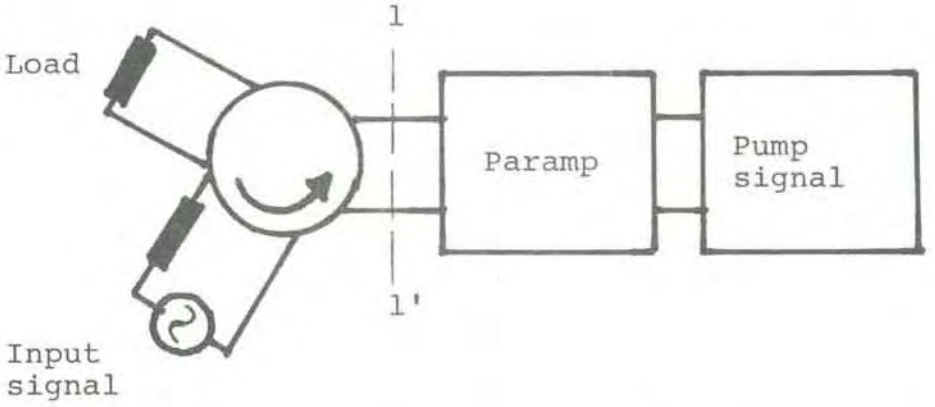

Figure 8.7 One-port parametric amplifier with circulator

The signal and the pump currents mix the varactor element to produce voltages and currents at many frequencies. We assume that the idling filter allows only the frequency

$$\omega_i = \omega_p - \omega_q \tag{8.25}$$

to flow. The idler current remixes with the pump current in the varactor diode and produces an amplified signal at ω_q at the output port 1-1'. The circulator is inserted to separate incoming and outgoing signals.

The power gain is given as:

$$G = \left| \frac{Z_{in} - R_g}{Z_{in} + R_g} \right|^2 \tag{8.26}$$

where Z_{in} is the impedance looking into the amplifier (1-1') and R_g is the characteristic resistance of the circulator. In assesing the noise properties the circulator loss must be taken into account. Also noise produced at the idler frequency will contribute to the

signal frequency noise. For an idler frequency $\omega_i=\omega_p-\omega_q$ the total amplifier noise figure is:

$$F = \left(1 + \frac{R_d}{R_L}\right)\left(1 + \frac{\omega_q}{\omega_p-\omega_q}\right) \qquad (8.27)$$

where R_L is the load resistance and R_d the series resistance of the varactor diode.

Literature:

Howson D.P., R.B.Smith - Parametric amplifiers, McGRAW-HILL, 1970

Shurmer H.V. - Microwave Semiconductor Devices, Pitman Publishing, 1971

EISCAT publications

F. du Castel, O. Holt, B. Hultqvist, H. Kohl and M. Tiuri:
A European Incoherent Scatter Facility in the Auroral Zone (EISCAT).
A Feasibility Study ("The Green Report") June 1971. (Out of print).

O. Bratteng and A. Haug:
Model Ionosphere at High Latitude, EISCAT Feasibility Study, Report No. 9.
The Auroral Observatory, Tromsö July 1971. (Out of print).

A European Incoherent Scatter Facility in the Auroral Zone, UHF System and Organization ("The Yellow Report"), June 1974.

EISCAT Annual Report 1976.(Out of print).

P.S. Kildal and T. Hagfors:
Balance between investment in reflector and feed in the VHF cylindrical antenna.
EISCAT Technical Notes No. 77/1, 1977.

T. Hagfors:
Least mean square fitting of data to physical models.
EISCAT Technical Notes No. 78/2, 1978.

T. Hagfors:
The effect of ice on an antenna reflector.
EISCAT Technical Notes No. 78/3, 1978.

T. Hagfors:
The bandwidth of a linear phased array with stepped delay corrections.
EISCAT Technical Notes No. 78/4, 1978.

Data Group meeting in Kiruna, Sweden, 18-20 Jan. 1978
EISCAT Meetings No. 78/1, 1978

EISCAT Annual Report 1977

H-J. Alker:
Measurement principles in the EISCAT system
EISCAT Technical Notes No. 78/5, 1978

EISCAT Data Group meeting in Tromsö, Norway 30-31 May, 1978
EISCAT Meetings No. 78/2, 1978.

P-S. Kildal:
Discrete phase steering by permuting precut phase cables.
EISCAT Technical Notes No. 78/6, 1978

EISCAT UHF antenna acceptance test.
EISCAT Technical Notes No. 78/7, 1978.

P-S. Kildal:
Feeder elements for the EISCAT VHF parabolic cylinder antenna.
EISCAT Technical Notes No. 78/8, 1978.

H-J. Alker:
Program CORRSIM: System for program development and software simulation of EISCAT digital correlator, User's Manual.
EISCAT Technical Notes No. 79/9, 1979.

H-J. Alker:
Instruction manual for EISCAT digital correlator.
EISCAT Technical Notes No. 79/10, 1979

H-J. Alker:
A programmable correlator module for the EISCAT radar system.
EISCAT Technical Notes No. 79/11, 1979.

T. Ho and H-J. Alker:
Scientific programming of the EISCAT digital correlator.
EISCAT Technical Notes No. 79/12, 1979.

S. Westerlund (editor):
Proceedings EISCAT Annual Review Meeting 1969. Part I and II,
Abisko, Sweden, 12-16 March 1979.
EISCAT Meetings No. 79/3, 1979.

J. Murdin:
EISCAT UHF Geometry.
EISCAT Technical Notes No. 79/13, 1979.

T. Hagfors:
Transmitter Polarization Control in the EISCAT UHF System.
EISCAT Technical Notes No. 79/14, 1979.

B. Törustad:
A description of the assembly language for the EISCAT digital correlator.
EISCAT Technical Notes No. 79/15, 1979.

J. Murdin:
Errors in incoherent scatter radar measurements.
EISCAT Technical Notes No. 79/16, 1979.

EISCAT Digital Correlator. TEST MANUAL.
EISCAT Technical Notes No. 79/17, 1979.

G. Lejeune:
A program library for incoherent scatter calculation.
EISCAT Technical Notes No. 79/18, 1979.